NASA Technical Memorandum 74094

EVALUATION OF THE THREE-DIMENSIONAL PARABOLIC FLOW COMPUTER PROGRAM SHIP

Y. S. Pan

JANUARY 1978

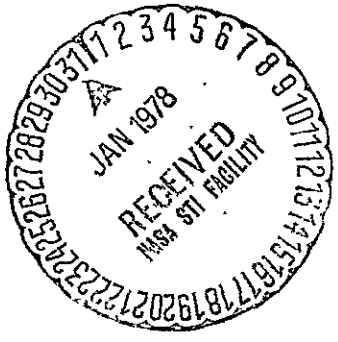

National Aeronautics and Space Administration

Langley Research Center
Hampton, Virginia 23665

EVALUATION OF THE THREE-DIMENSIONAL PARABOLIC FLOW COMPUTER PROGRAM SHIP

Y. S. Pan*

SUMMARY

Design of supersonic combustors for scramjet engines requires significant detailed information about the flow field. Traditional approaches based mainly on experimentation have been limited by difficulties in the acquisition of meaningful data. Recent advances in computational capabilities have made it possible to begin to predict complex flow fields in the combustor. Such analytical approaches could supplement the traditional approach by eliminating the need for some of the costly experimental parameter studies.

A three-dimensional parabolic flow program designed for supersonic combustors is evaluated to determine its capabilities. The mathematical foundation and numerical procedure are reviewed; simplifications are pointed out and commented upon. The program is then evaluated numerically by applying it to several subsonic and supersonic, turbulent, reacting and non-reacting flow problems. Computational results are compared with available experimental or other analytical data. Good agreements are obtained when the simplifications on which the program is based are justified. Limitations of the program and the needs for improvement and extension are pointed out. The three-dimensional parabolic flow program appears to be potentially useful for the development of supersonic combustors.

---

*National Research Council Senior Resident Research Associate, NASA Langley Research Center.

INTRODUCTION

Design of supersonic combustors for scramjet engines requires significant detailed information about the flow field. The traditional approach to combustor development has been mainly based on expensive, cut-and-try experimentation. Because of the highly turbulent and high-temperature environment in supersonic combustors, the acquisition of meaningful data is extremely difficult. Due to recent advances in computational techniques and computer capabilities, however, it is now possible to make computations for three-dimensional mixing-reacting turbulent flow fields in combustors. Analytical predictions for guiding the supersonic combustor development and experimentation will be very valuable to reduce costly hardware iterations based purely on experimentation.

Several numerical approaches (for example, refs. 1-3) are available at present to predict three-dimensional turbulent mixing flow fields. Based on published results in the technical literature, the approach (ref. 1) developed by Spalding's group at Imperial College seems to be the most widely used. Satisfactory results have been obtained from their computer codes for many three-dimensional flow problems (for example, refs. 4-7). The three-dimensional parabolic flow computer program SHIP* (ref. 8) has been developed by Spalding's group for the NASA Langley Research Center and is used along with programs developed elsewhere for predicting combustor flow fields. This program is the subject of the present evaluation.

---

*SHIP (Supersonic Hydrogen Injection Program) is a later version of and supersedes HISS (Hydrogen Injection into a Supersonic Stream, ref. 9)

The general philosophy of the approach of Spalding's group has been reflected in many of their publications (for example, refs. 4, 10-13). That philosophy is to produce useful engineering results without being overly rigorous in formulations, and unduly time consuming or expensive. Therefore, in their approach, many assumptions and/or simplifications are used to achieve efficiency in both computer storage and computing time; however, some of them are difficult to justify rigorously. The accuracy and applicability of such an approach can only be established by testing the computations against experimental data or against computations produced by a more rigorously formulated approach. Some of the results of such an evaluation are given in this paper.

The present paper is organized as follows. The fundamental formulation and numerical procedure are outlined and reviewed in this paper. Assumptions and/or simplifications are pointed out and commented upon. The computer program is then applied to several reacting and nonreacting, turbulent and nonturbulent flow problems and results are compared with available experimental data or to other computations. Finally, the overall capabilities of the program are discussed. Additional development and needs for extensions related to the supersonic combustor flow field predictions are pointed out.

SYMBOLS

The International System of Units (SI) is used in this paper.

A	constant, eq. (5)
A,B	coefficients of difference equation, eq. (2)

C_1, C_2, C_D	constants associated with turbulence model
C_f	coefficient of shear stress
D	damping factor defined by eq. (5)
d	injector diameter
f	mass concentration
H	total enthalpy or shape factor of turbulent boundary layer, δ^*/θ
k	turbulence kinetic energy
ℓ	turbulence length scale
ℓ_m	mixing length
M	Mach number
p	pressure
Pr	Prandtl number
Re	Reynolds number
S	source term, eq. (1)
s	jet spacing
Sc	Schmidt number
T	temperature
u, v, w	velocity components
W_1, W_2	free-stream velocities of two mixing streams, eq. (6)
w^+	nondimensional velocity of turbulent boundary layer, eq. (3)
x, y, z	rectangular coordinates
y^+	nondimensional coordinate in turbulent boundary layer, eq. (3)
z_j	injection location
Γ	exchange coefficient

δ	boundary layer or mixing layer thickness
δ^*	displacement thickness
δ^{**}	energy thickness
ε	turbulence dissipation energy rate
Θ	momentum thickness
κ	constant, eq. (4)
λ	constant, eq. (4)
μ	viscosity
ξ	nondimensional coordinate in mixing layer, eq. (6)
ρ	density
σ	spreading constant of mixing layer
τ	shear stress
ϕ	general dependent variable, eq. (1)

Subscripts:

eff	effective
E, W, S, N	east, west, south, and north, respectively
ℓ	laminar
o	total
p	particular node or pitot condition
t	turbulent
w	wall
ϕ	general dependent variable

REVIEW OF THE COMPUTATIONAL APPROACH

In this section the three-dimensional parabolic flow computer program, SHIP, developed for the NASA Langley Research Center (ref. 8), is introduced. Its theoretical foundation, numerical procedure, and simplifications are discussed.

The computer program is designed for calculating three-dimensional, turbulent, reacting, parabolic flows (either external or internal). The flow field considered in the program is a flow confined in a rectangular parallelepiped; any of the four lateral boundaries can be a wall, a symmetry plane, or a free-stream condition along a given surface. For walls, the distance of each wall from a reference plane may be specified as an arbitrary smooth function of distance along the main flow direction. The main flow can be either subsonic or supersonic. Variable specific heats are used for different species in the flow and the mixture satisfies the equation of state of a perfect gas; four equilibrium chemical reactions are allowed.

The SHIP program was developed based on the Eulerian formulation in a rectangular coordinate system (x, y, z) with the z-axis in the main flow direction. The mean flow velocity components (u, v, w), pressure (p), density (ρ), total enthalpy (H), and hydrogen mass concentration (f) of the three-dimensional turbulent mixing-reacting flow are governed approximately by the Navier-Stokes equations together with the equation of state for perfect gases and a specie equation. To account for the turbulence, the laminar (molecular) viscosity (μ_ℓ) is replaced by an effective viscosity

($\mu_{eff} = \mu_\ell + \mu_t$), and the laminar (molecular) Prandtl number Pr_ℓ and Schmidt number Sc_ℓ are replaced by their empirical effective values to be discussed later. The turbulent viscosity (μ_t) is determined by way of a "k-ε" two-equation turbulence model. Analogous to the molecular viscosity defined in the kinetic theory, the turbulent viscosity is related to the density, a turbulence velocity scale (e.g. square-root of the turbulence kinetic energy k) and a turbulence length scale ℓ. At high Reynolds numbers, ℓ is proportional to $k^{3/2}/\varepsilon$, with ε the turbulence dissipation energy rate. Hence $\mu_t = C_D \rho k^2/\varepsilon$ with C_D being an empirical constant, and k and ε are determined by a set of transport equations with several additional empirical constants (ref. 14).

One of the important simplifications for the development of the programs is the parabolic flow assumption (ref. 4). When there exists a predominant flow direction, when the diffusion of mass, momentum, energy, etc., can be neglected in that direction, and when the downstream pressure field has little effect on the upstream flow field, the coordinate in the main flow direction (z) becomes a "one-way" coordinate. The set of governing equations reduces mathematically to the parabolic type, and can be numerically solved in succeeding cross-stream (x-y) planes in the main-stream direction. Because of this simplification, a three-dimensional program requires only two-dimensional computer storage. Consequently, computer storage and running time are greatly reduced. It should be noted that the classical Prandtl boundary layer flow is a two-dimensional parabolic flow, but, unlike the simplification used here, the Prandtl

boundary layer equations can be justified rigorously by an order of magnitude or a perturbation estimation.

The simplified governing equations for the present parabolic flow can be represented by the following general differential form,

$$\frac{\partial}{\partial z}(\rho w\phi) + \frac{\partial}{\partial x}(\rho u\phi - \Gamma_\phi \frac{\partial \phi}{\partial x}) + \frac{\partial}{\partial y}(\rho v\phi - \Gamma_\phi \frac{\partial \phi}{\partial y}) = S_\phi \qquad (1)$$

where ϕ is a general dependent variable and Γ_ϕ is a general exchange coefficient. When $\phi = 1$, u, v, w, H, f, k, or ε, equation (1) corresponds, respectively, to the continuity, three components of momentum, energy, concentration, turbulence kinetic energy, or turbulence dissipation energy rate equation. On the left-hand side of equation (1), the first term represents convection in the main flow (z) direction, and the second and third terms represent, respectively, the sum of convection and diffusion in the lateral x and y directions. The term S_ϕ on the right-hand side is a source term which includes all other terms left from each of the simplified differential equations, such as the pressure gradient terms in the three momentum equations. The appropriate exchange coefficients Γ_ϕ and source terms S_ϕ for variables ϕ corresponding to different conservation equations are listed in Table I. (Note that some of the source terms are different from those in refs. 8 and 9, and have been improved during the present evaluation.) The general effective exchange

coefficient is composed of two parts, a turbulent and a laminar; i.e.

$$\frac{\mu_{eff}}{Pr_{eff,\phi}} = \frac{\mu_t}{Pr_{t,\phi}} + \frac{\mu_\ell}{Pr_{\ell,\phi}}$$

where $Pr_{t,\phi}$ and $Pr_{\ell,\phi}$ are, respectively, the turbulent and laminar Prandtl numbers. The values of Pr_t, Pr_ℓ and the constants, C_1 and C_2 in Table I are usually determined empirically (for example, ref. 14).

The numerical formulation is based on a finite-difference form of equation (1). A "staggered" grid system is used in the x-y plane (ref. 8). The advantage of such a system is that velocity components u and v are stored just at the point (midway between the two neighboring nodes) at which they are needed for the calculation of the convection, and the pressures are stored so as to make it easier to calculate the pressure gradients for calculating u and v. Thus, control volumes at each node are different for u and v as compared with w and the other ϕ's. By taking volume integrals of equation (1) over respective control volumes, a set of difference equations can be obtained. The volume integrations of the terms $\frac{\partial}{\partial z}(\rho w \phi)$ and S_ϕ in equation (1) are performed by assuming that the values of ϕ, ρ, and w at a node point P are constant over the entire control volume. The term $\frac{\partial}{\partial z}$ contains the difference of values at stations z and $z + \Delta z$. The volume integrals of the other two terms in equation (1) give rise to the surface integrals of the convective and diffusive

fluxes across the boundaries of the control volume. A proper representation of these terms is essential to the convergence of numerical computation. To provide numerical convergence and accuracy, a "hybrid" scheme is used. This scheme is a combination of central and upwind differences; the rationale of this scheme and some experience with its use are described in references 10 and 15. When the integrations of various terms in equation (1) are expressed in the manner described above, the following general form of the difference equations is obtained at an arbitrary node P,

$$\phi_P = A_N\phi_N + A_S\phi_S + A_E\phi_E + A_W\phi_W + B \qquad (2)$$

Here, the values of ϕ's pertain to station $z + \Delta z$ and the values of A's and B pertain to station z. The subscripts N, S, E, and W denote, respectively, the neighboring north, south, east, and west nodes. The derivation of equation (2) from equation (1) is given in the Appendix.

In the present program, the set of difference equations (2) together with other auxiliary equations are not solved point-by-point simultaneously, but by a so-called SIMPLE (for Semi-Implicit Method for Pressure Linked Equations) method (ref. 4). Although the flow problem is highly nonlinear, an economical noniterative procedure is followed. The three velocity components are solved from their respective (ϕ = u, v, w) difference equations in terms of a guessed pressure field. This guessed pressure field

is then corrected by the continuity equation, i.e. equation (1) with $\phi = 1$. The pressure correction satisfies a difference equation similar to equation (2). After the guessed pressure field and three components of velocity field have been corrected by the pressure correction, the difference equations (2) for H, f, k and ε are solved sequentially. Temperature, density, mass concentrations of species and other auxiliary quantities are determined noniteratively by their appropriate relations.

By knowing appropriate boundary conditions, each difference equation of equation (2) can be solved readily by several computer algorithms. However, it is usually adopted by the Spalding group that equation (2) is solved in a line-by-line iterative fashion by the successive use of a standard tri-diagonal matrix algorithm in the x and y directions. Great economy of computer time has been found by using this procedure (ref. 11).

One additional feature of the programs is the handling of boundary conditions for these difference equations. The boundary conditions are specified by the values of appropriate fluxes across the boundaries. For a free or symmetry boundary, fluxes are automatically set to zero. For solid walls, to avoid using a large number of grid points to compute steep gradients in the sublayers, simplifications are employed. On such boundaries, the well-known (turbulent boundary layer) wall functions are used at near-boundary grid points located in the turbulent flow region. Moreover, the wall shear in the wall functions is replaced by the local Reynolds stress which, in turn, is related to the local turbulence kinetic energy in an equilibrium high Reynolds number turbulence flow. Near

the intersections of two walls, the corner flows are not specially treated.

In the SHIP Program, the wall boundaries are allowed to vary along the main flow direction; the coordinates chosen are no longer orthogonal. However, it is stipulated that two of the coordinates (x, y) are maintained mutually orthogonal throughout the flow field, while the third (z) axis is permitted to depart from orthogonality with respect to the other two. The error thus introduced is of the order of the tangent of the angle of departure from orthogonality.

As reviewed above, the capabilities and limitations of the present parabolic flow programs depend primarily on the simplifications introduced and on the turbulence modeling. At present, it is believed that the "k-ε" two-equation turbulence model with appropriate constants is suitable for high Reynolds number flows. In low Reynolds number flow regions, such as near a wall or in a transition region, the turbulence model requires some special attention.

Simplifications related to the development of the present program can be generally summarized and classified as follows:

Simplifications which limit the range of the application of the program. - They are: (1) the parabolic flow assumption; and (2) the non-orthogonality of coordinates. The former excludes computations of flows with recirculation and/or with large pressure effects from downstream. The latter excludes computations with large variations of wall geometries.

Simplifications which affect the accuracy of the program. - They are the noniterative SIMPLE procedures and the iterative procedure of solving difference equations. The accuracy of the program due to these simplifications may be improved by increasing grid numbers, using smaller forward steps and/or increasing numbers of iterations.

Simplifications which may affect the local flow field. - One such simplification is the application of wall-functions at near-boundary grid points for solid boundaries. As described previously, the wall shear in the wall functions is approximated by using the local Reynolds stress which, in turn, is related to the local turbulence kinetic energy in an equilibrium high Reynolds number turbulent flow. For practical applications, the local Reynolds stresses at the near boundary grid points are not equal to the wall shear if the points are too far from the wall boundary; on the other hand, the high Reynolds number relationship between the local Reynolds stress and turbulence kinetic energy is not appropriate at the near boundary grid points if they are too close to the wall (ref. 14). Hence, using such a simplification in the wall function, the program may not yield accurate wall shear stresses and heat transfer. Similarly, using such a simplified wall boundary condition, the program may not predict accurate flow fields near the wall. However, this flow field may be improved by using correct wall shear and/or by applying low Reynolds number corrections in the wall functions.

The last simplification is not related to the development of the programs, but is in the application. That is how to specify the conditions at the initial station. Mean flow quantities, such as velocity components,

pressure and density, are usually measured and relatively easy to specify. The initial turbulence kinetic energy and dissipation energy rate are usually not measured and must be estimated for each computation. Currently, the turbulence kinetic energy and dissipation energy rate are estimated by means of the mixing-length hypothesis. The effects of such an estimate on some flow fields are significant and will be given in the next section along with comparisons of computational results and experimental data.

APPLICATION OF THE COMPUTER PROGRAM

The parabolic flow computer program SHIP has been applied to several flow fields. The objectives of such applications are: (1) to test the accuracy against available experimental data or other computational results; (2) to establish or verify the values of empirical constants associated with the "k-ε" two-equation turbulence model; and (3) to determine the limitations of this program. Numerical computations were performed for the turbulent boundary layer flow of Wieghardt (ref. 16), the turbulent mixing layer flow of Brown and Roshko (ref. 18), compression and expansion of supersonic flow in a two-dimensional duct, mixing of a jet normal to a supersonic stream (ref. 22), and supersonic combustion and mixing of a hydrogen wall jet in a duct (refs. 23, 24).

Turbulent Boundary Layer Flow

The two-dimensional turbulent boundary layer over a flat plate is perhaps the simplest and most-examined turbulent flow in the presence of a solid boundary. Such a flow satisfies the parabolic flow assumption,

and the program should be applicable. Wieghardt's flat plate flow examined in the 1968 Stanford Conference (ref. 16) is chosen as typical of the standard flat-plate boundary layer. The free-stream flow velocity was 33 m/sec and the model was a waxed-plywood plate with a blunt leading edge fitted with a small trip wire. The mean-velocity profiles were measured by a probe rake at several downstream stations. The first profile at z = 0.087 m is probably at about the minimum Reynolds number for turbulent flow. The tunnel turbulence level was about 0.25 percent and an average kinematic viscosity was about 0.151 cm^2/sec.

Since the present program cannot predict boundary layer transition and the present two-equation turbulence model is not appropriate in low Reynolds number flows, computations by the program are started at z = 0.187 m ($Re \cong 4.1 \times 10^5$) and Wieghardt's measurements at that station are used for the initial conditions. Pressure, density, and temperature are assumed to be constant across the boundary layer and equal to their free-stream values. The ten initial velocity measurements across the boundary layer are matched by the following wall function near the wall ($y^+ < 50$):

$$w^+ = y^+ \qquad \text{for} \quad 0 \leq y^+ < 11.4 \tag{3a}$$

$$w^+ = 5.5 + 2.5 \ln y^+ \qquad \text{for} \quad 11.4 \leq y^+ < 50 \tag{3b}$$

Here $w^+ = \dfrac{w}{\sqrt{\tau_w/\rho}}$ and $y^+ = \dfrac{y\sqrt{\tau_w \rho}}{\mu_\ell}$ are, respectively, the nondimensional

velocity and coordinate perpendicular to the wall; τ_w is the wall shear. The initial turbulence kinetic energy and dissipation energy rate are estimated from the initial velocity profile by the mixing length hypothesis (ref. 17). The mixing-length ℓ_m is defined as follows,

$$\ell_m = \lambda\delta \quad \text{for} \quad y \geq \frac{\lambda}{\kappa}\ \delta \tag{4a}$$

$$\ell_m = \kappa y D \quad \text{for} \quad y < \frac{\lambda}{\kappa}\ \delta \tag{4b}$$

where

$$D = 1 - \exp\left[-y(\tau\rho)^{1/2}/\mu_\ell A\right] \tag{5}$$

is a damping factor. δ = 0.005m is the boundary thickness at the station z = 0.187 m and the empirical constants λ = 0.09, κ = 0.435, and A = 26.

Computations were performed to downstream stations with empirical Spalding constants associated with the "k-ε" two equation turbulence model (ref. 8): C_1 = 1.44, C_2 = 1.92, C_D = 0.09, laminar Prandtl number Pr_ℓ = 0.7 and turbulent Prandtl numbers $Pr_{t,\phi}$ = 1.0 for ϕ = v, w, H and k, and 1.3 for ϕ = ε. At the near boundary grid points located just outside the sublayer, a constant wall shear coefficient (at z = 0.187 m) C_f = 0.00424 was used in the wall function. Results of velocity profiles at z = 0.187, 0.287,

0.387, 0.487, and 0.637 m are compared with Wieghardt's data in figure 1. The integral parameters, displacement thickness δ^*, momentum thickness θ, energy thickness δ^{**} and the shape factor H $(= \delta^*/\theta)$ are compared with Wieghardt's data in figure 2. Comparisons of computations with experiments in figures 1 and 2 are in excellent agreement.

Computations were also performed with the same set of empirical constants but with Reynolds stresses replacing the wall shear in the wall function. A typical velocity comparison (at $z = 0.487$ m) is shown in figure 3. The agreement with experimental data is not as good as that of the previous calculation. Due to the disagreement in velocity profiles, the comparisons of the integral parameters are also bad. This kind of disagreement should be expected, since the development of the turbulence is due to the presence of the wall; i.e. the wall boundary conditions dominate the boundary layer flow field. This comparison sustains the comment made about the wall boundary condition in the previous section.

Turbulent Mixing Layer Flow

The two-dimensional turbulent mixing layer is the simplest turbulent mixing flow without influence from a wall. Recent experiments by Brown and Roshko (ref. 18) are used as the present test cases. The objective is to compare the mixing profiles of the present computation with those of the experiments.

Brown and Roshko's experiments were conducted for mixing of two streams separated upstream by a splitter plate. The streams having different velocities but the same density or different densities were mixed. Profiles

of velocities and densities were reported at several downstream stations from the trailing edge of the splitter plate. Since a trailing edge flow is theoretically not a parabolic flow, the present computations were then started from the first station of their measurements. The initial turbulence kinetic energy and dissipation energy rate were estimated by the mixing-length hypothesis (ref. 17). The mixing-length ℓ_m is related to the thickness of the mixing layer δ, which, at a station z, is the distance between two streamlines y_1 and y_2 defined by $[W_1-w(y_1)]/(W_1-W_2) = 0.1$. and $[W_1-w(y_2)]/(W_1-W_2) = 0.9$, respectively. For two-dimensional plane flows, $\ell_m = 0.125\ \delta$ (ref. 19).

Mixing of the two airstreams with different velocities (10 and 1.43 m/sec) is considered first. The measured velocity data at the first station (z = 0.0254 m) and the initial profile for the computation are shown in figure 4; the thickness of the mixing layer at this station is 0.0038 m. Since the distance of this station from splitter plate is about 1000 times the momentum thickness of the boundary layer leaving the plate, the velocity profile has already exhibited the similar nature of the free mixing layer. As noted in ref. 18, the virtual origin (z_0) of the similar mixing layer is about 6.35×10^{-3} m upstream of the trailing edge. In the computation, the values of following empirical constants associated with the "k-ε" two-equation turbulence model were used (ref. 19): $C_1 = 1.44$, $C_2 = 1.92$, $C_D = 0.09$, $Pr_\ell = 0.7$, $Pr_{t,\phi} = 1.0$ for ϕ = v, w, and k, 1.3 for $\phi = \varepsilon$ and 0.5 for ϕ = H. Pressure, density, and temperature were taken to be constants across the mixing layer at the initial station.

Computational results of velocity at downstream stations (z = 0.0508, 0.0635, 0.0762 and 0.0889 m) are compared with the experiments in figure 5. Comparisons are in good agreement except some discrepancies do occur at the edges of mixing layer where the experimental data deviate from the computational results possibly due to large structures of the turbulence. A computation was also performed by fitting the initial velocity with a similar profile (ref. 20),

$$w = \frac{W_1 + W_2}{2}\left[1 + \frac{W_1 - W_2}{W_1 + W_2}\,\mathrm{erf}\ \xi\right] \tag{6}$$

where W_1 = 10 m/sec, W_2 = 1.43 m/sec; erf (ξ) is the error function with the argument $\xi = \sigma(y-y_0)/(z-z_0)$ and σ = 13.5, $y_0 = -2.9 \times 10^{-4}$m. The results are indistinguishable from the previous computations, so the computations are not shown separately in figure 5.

The second test case is the mixing of flows with different media (N_2 and He) and with different velocities (10 and 3.78 m/sec, respectively, for N_2 and He). The velocity and density data at the first station (z = 0.0254 m) and the initial profiles for the computation are shown in figure 6 (with z_0 = -0.0254 m). The thickness of the mixing layer at this station was 0.0031 m. In this computation, the same empirical constants as the air-air mixing case were used; in addition, the turbulent Prandtl number Pr_t = 0.5 for the concentration was used in the specie equation. Computational results are compared with the corresponding experimental data at several

downstream stations (z = 0.0508, 0.0762 and 0.1016 m) in figure 7. Agreements are good for the velocity profiles, but not as good for the density profiles.

The discrepancies in the density comparison led to the calculation of another mixing layer problem; i.e., N_2 and He with velocities 1.43 and 10 m/sec, respectively. Again, the velocity and density data at z = 0.0254 m were used as the initial conditions; they are shown in figure 8. Since the thickness of the velocity and density mixing layers are not equal, the algebraic mean thickness was used (δ = 0.0064 m). Computational results of velocity and density are plotted in figure 9 to compare with experimental data at different downstream stations (z = 0.0508, 0.0635, 0.0762 and 0.0889 m). Again, the agreements are good for the velocities; the comparisons of densities are not good, especially in the part of mixing layer with higher density.

Computations of these mixing layers have shown that the estimate of initial turbulence kinetic energy and dissipation energy rate has a significant effect on the downstream mixing profiles. For mixing of streams with equal densities, the Prandtl mixing-length hypothesis with a constant mixing length seems to be appropriate for such an estimate. For mixing of streams with different densities, however, such an estimate together with the "k-ε" two-equation turbulence model does not predict the same similar nature of the mixing layer as the experiment did and, consequently, yields discrepancies. Different comparisons can be obtained by trying different estimates of the initial turbulence kinetic energy. For example, by

assuming a mixing-length which varies with density (i.e., $\ell_m = \frac{0.125}{976} \rho^5 \delta$) in the last test case, a better agreement with the experiment was obtained. A typical comparison of such results at z = 0.0889 m is shown in figure 10.

At present, there are no general methods which are also simple (like the Prandtl mixing-length hypothesis) to estimate "correct" initial turbulence kinetic energy and dissipation energy rate for use with the "k-ε" two-equation turbulence model in a medium with large density variations. For the present mixing layer problem, two approaches may be possible to provide the initial data of the turbulence kinetic energy and dissipation energy rate. First, since the mixing layers at and downstream of the first station of measurements are already similar, a similarity consideration could be used to reduce the set of governing (partial differential) equations to ordinary differential equations. A "correct" and also similar, turbulence kinetic energy or dissipation energy rate profile could then be related to other known flow variable profiles and their derivatives at that station. Second, the "correct" turbulence kinetic energy (and other flow variables) as the initial conditions to the present parabolic flow program may be obtained by directly solving an elliptic-type turbulent-trailing-edge flow problem. Since the mixing-length hypothesis is appropriate for the medium on either side of the splitter plate, the elliptic solution should be free of uncertainties to determine the upstream boundary conditions of the turbulence kinetic energy and dissipation energy rate.

Compression and Expansion of Supersonic Flow

In this section, supersonic flow in a two-dimensional channel with variable heights is computed by the SHIP Program. The objective is to demonstrate how compressions and expansions are handled by the parabolic flow computer program.

The geometry of a two-dimensional channel and the wave pattern in the channel are sketched in figure 11. The upper and lower walls of the channel are parallel and 0.2 m apart initially. At z = 0.1 m, the lower wall is deflected by an angle α(= 3.366°) into the flow; at z = 0.3 m, the lower wall is deflected away from the flow by the same angle α. The flow is uniform initially with M = 1.5, p = 0.1 MN/m^2, and T = 294 K. Computations are performed for two cases: one with zero laminar viscosity and one with a variable laminar viscosity. In both cases, however, the turbulence viscosity and kinetic energy are set small ($\mu_t \simeq 10^{-30}$) and kept constant. No-slip boundary conditions at walls are used in both cases.

Computational results of pressures at the upper and lower walls are plotted in figure 12. For comparison, the pressures computed by a two-dimensional inviscid shock fitting method (ref. 21) are also plotted*. It may be noted that the shock fitting method employs a finite-difference numerical scheme; however, the locations and strengths of the shock discontinuities are treated explicitly. By comparing the computational results

*Acknowledgment is made to J. P. Drummond for his help in providing data by use of Program SEAGULL.

of two methods, the results of the SHIP program show delays in pressure responses at both shocks and expansion corners. This kind of discrepancy is due to the finite-difference numerical scheme and the parabolic flow assumption. The former causes the smear of shocks and expansions at corners, whereas the latter prohibits transmission of disturbances to upstream points even in the subsonic flow region near the wall. Since a disturbance can transmit laterally (and to downstream) by diffusion and convection, pressures in the laminar case show slightly better comparisons with those of the shock fitting method than those of the zero-viscosity case in the compression regions.

Pressure variations across the channel at three stations (z = 0.24, 0.35 and 0.48 m) are shown in figure 13. Comparisons of the two present computations with the shock fitting method are reasonably good except directly behind a shock or at an expansion corner due to the reasons stated above.

Comparisons in figures 12 and 13 also show that a better agreement is obtained in regions with gradual pressure variations than with sharp changes. In the actual turbulent flow near a wall, shocks are smeared by large diffusive effects, so the pressure changes are usually more gradual than in the inviscid flow. Therefore, it is believed that the prediction of the present program will be in better agreement with experiments in a supersonic turbulent channel flow than with the results of an inviscid flow-field calculation.

The computational results discussed above were obtained by using 60 grid points equally spaced across the two-dimensional channel and the

forward step size being equal to 1/40 of the channel height. By varying the number of grid points and the step size, it was found that the numerical results do not have appreciable changes for grid points over 30 and for the step size less than 1/40 of the channel height. However, in the inviscid computations, the steep pressure variation across shocks can be improved by taking smaller forward step size.

Mixing of Jet Normal to a Supersonic Stream

In this section, the parabolic flow computer program is applied to a case of three-dimensional mixing of cold hydrogen injected normal to a supersonic airstream. Such experiments were reported in reference 22. The flow field and the arrangement of injectors at the injection station (z_j) are sketched in figure 14. Experimental surveys of flow field were made at several downstream stations ($(z-z_j)/d$ = 7, 30, 60, 120, and 240 with the injector diameter d = 1.026 x 10^{-3}m) for two injector-arrangements (s/d = 6.25 and 12.5).

Recognizing the occurrence of recirculating flow regions directly downstream of the injectors, the parabolic flow program was used to compute the flow field far downstream of the injectors where the recirculation is not present. The y-z plane was centered on the central jet; the two mid-planes ($\frac{x}{d} = \pm 3.125$ for the case of s/d = 6.25) between the central jet and its neighbors were chosen as the two "symmetric" boundaries. The other two boundaries were the wall (y = 0) and a free-stream boundary (y = H = 0.1 m). The experimental data (ref. 22) at the station 30 injector diameters downstream of the injection were used as initial conditions.

Since measurements were taken mostly along the symmetric plane (x = 0) at that station, very few measurements are available at other locations at that station. In order to make the experimental data fit onto the initial data (x,y) plane with 12 x 25 grid points, some flow quantities were assumed at several additional locations including the boundaries. By using a cubic spline interpolation routine, initial data at the 12 x 25 grid points were obtained. Typical initial profiles of w, T, f and p at x/d = 0 and 2.19 are shown in figure 15; the corresponding experimental data at x/d = 0 are plotted for comparison.

Because of the uncertainty due to the large number of assumed initial values, the computation was not intended for detailed comparisons of the accuracy with experiments. Thus, for simplicity, the initial turbulence kinetic energy and dissipation energy rate were assumed to be zero, and the initial lateral velocity components were also taken to be zero. Computations were then carried to the downstream stations. Typical profiles of w, T and f at x/d = 0 and 2.19 are shown in figures 16 and 17 for the stations $(z-z_j)/d$ = 60 and 120, respectively. The available experimental data at x/d = 0 are also plotted. The comparisons show a general qualitative agreement between the experiments and computations.

A similar computation for the case of s/d = 12.5 was also performed. Typical results of w, T and f at x/d = 0 and 5.0 and their comparisons with corresponding experiments at x/d = 0 are shown in figure 18. Again, the computations are in qualitative agreement with the experiments. To make detailed comparisons of three-dimensional computations with experiments,

a complete survey of flow fields is necessary and should be carefully planned.

Supersonic Combustion and Mixing of Hydrogen in a Duct

Most of turbulent reacting (combustion) experiments were conducted for axisymmetric configurations which are not appropriate for the direct application of the present program because of the rectangular coordinate system. Burrows and Kurkov (refs. 23, 24) performed supersonic combustion of hydrogen and turbulent mixing tests in a rectangular duct and made probe measurements of temperature, pressure, and composition within the test section. Such measurements are useful to test the present program, especially the simplification of equilibrium chemical reactions.

The test section of the experiment is sketched in figure 19. A high pressure gas generator supplied either Mach 2.44 vitiated air at static temperature of 1270 K or Mach 2.44 inert gas of 1150 K and a static pressure of 0.1 MN/m^2. Hydrogen also at 0.1 MN/m^2 was injected at Mach 1 (at $z = 0$) into the flow in the heat sink combustion duct from a stepped-wall injector. The cross-section of the duct expanded linearly from 5.10 by 9.38 centimeters at $z = 0$ to 5.10 by 10.48 centimeters at the exit ($z = 35.6$ cm) to compensate for boundary layer buildup. The total temperature and composition profiles were recorded at the injection step and at the exit station; in addition, pitot pressure profiles also recorded at the exit station. Detailed test conditions, probe measurements and some deduced flow variables like velocity and temperature were reported in references 23 and 24.

In the application of the SHIP program, the velocity and temperature from references 23 and 24 at the injection step ($z = 0$) were used as the initial data which were assumed uniform in the transverse (x) direction. Pressure and composition were taken to be uniform at the initial station. At the walls, constant wall temperature of 298 K was assumed and heat transfer was allowed across the wall boundaries. Both two- and three-dimensional computations were performed. In the two-dimensional computation, the top (north) and bottom (south) boundaries were walls and the east and west boundaries were symmetric surfaces. In the three-dimensional computation, all boundaries were kept the same as the two-dimensional computation except that the west boundary ($x = 0$) was changed to a wall.

Initial turbulence kinetic energy and dissipation energy rate were estimated based on the mixing-length hypothesis. Due to the two-dimensional nature of the initial data, two-dimensional turbulent boundary layers were assumed adjacent to the walls; the local mixing length was then related to the corresponding boundary layer thickness. (See eqs. (4a) and (4b).) In the wall jet, two-dimensional velocity and temperature variations were assumed and the thickness of boundary layer was taken to be the half of the wall-jet height (0.2cm). In the test section, the boundary layer thickness was assumed to be 0.4 cm. It might be noted that the measurement of total temperature profile (in the y-direction) at the injection step indicated the variation in a thick layer of 2 cm. It was not clear whether the variation in this thick layer was entirely due to the turbulent boundary layer or due to other effects such as wave interactions in the duct. Furthermore, no information about flow variations were available in the

transverse direction (the small dimension of the duct) which could help to estimate the boundary layer thickness. The estimate of initial mixing length and turbulence kinetic energy based on this thick layer (2.0 cm), however, was found to result in too much turbulent mixing at downstream in both combustion and mixing cases.

Computations were performed with the values of the following empirical constants associated with the "k-ε" two equation turbulence model: $C_1 = 1.44$, $C_2 = 1.92$, $C_D = 0.09$, $Pr_\ell = 0.7$, $Pr_{t,\phi} = 1.0$ for ϕ = u, v, w, and k, 1.3 for $\phi = \varepsilon$, and 0.5 for ϕ = H and f. Computational results at the exit station (z = 35.6 cm) were compared with the experimental data in fig. 20 for the combustion case and in fig. 21 for the pure mixing case. Comparisons show generally good qualitative agreements. However, some discrepancies do exist in these comparisons, for example the composition profiles in fig. 20a. Such discrepancies may be attributed to the simplification of equilibrium chemical reactions, the uncertainties associated with the initial mixing length and turbulence kinetic energy, and the two-dimensional initial data. It has been shown, for example, that nonequilibrium chemistry can shift the concentration profiles (ref. 25). Variation of initial mixing length could also alter the shape of computational profiles. Furthermore, the estimate of initial turbulence kinetic energy by means of the mixing length hypothesis would be significantly different if the initial flow fields were three-dimensional. From the geometry of the duct, the turbulent boundary layers at two side-walls may contribute significant mixing effects because of the smaller transverse dimension of the duct. The two-dimensional flow field at the initial station, however,

has resulted in only moderate differences between the three- and two-dimensional computations. Because of the absence of chemical reactions, the composition profiles of the pure mixing case (fig. 21a) are in better agreement than those in the combustion case (fig. 20a). In addition, it may be noted that combustion builds up pressure in the combustor duct. The pressure propagates upstream through the subsonic boundary layer adjacent to the wall and affects the supersonic upstream flow field. Such a supersonic-subsonic interaction is not considered in the present parabolic flow program; its effects are difficult to estimate in the present comparison.

DISCUSSION OF THE PROGRAM CAPABILITIY

The theoretical formulation and numerical procedure of the parabolic flow computer program SHIP have been reviewed. In order to achieve economical operation of the program, many mathematical and physical simplifications were introduced in its development. Some simplifications affect only the accuracy of the numerical result; others limit the application of the program. A numerical evaluation of the program has been performed for several two- and three-dimensional turbulent, reacting and nonreacting flow fields. Generally good numerical predictions are obtained when the simplifications on which the program is based are justified.

The results of application of the present program to three-dimensional reacting and nonreacting flow fields are not conclusive because of the lack of detailed three-dimensional measurements. However, the program is capable of predicting three-dimensional flow fields with qualitatively

good agreement with available experimental measurements. Quantitatively accurate predictions are, in general, dependent on the proper estimate of the initial turbulence kinetic energy and dissipation energy rate and, in reacting flows, on the "correct" turbulence-chemical reaction model. For chemical reactions in turbulent flow, studies are still needed to define a "correct" turbulence-chemical reaction model, and such studies should be conducted in a flow field of simpler geometry, e.g. two-dimensional planar or axisymmetric flow (ref. 26). With confidence in the turbulence-chemical reactions, such a model could be incorporated into the present program.

The difficulties associated with the estimate of initial turbulence kinetic energy and dissipation energy rate are almost proportional to the complication of the flow field at the initial station. The complication of the initial flow field is usually due to the occurrence of the recirculating or "elliptic" flow field in the very near field; for example, the recirculation immediately downstream of the normal injection, and the "elliptic" flow near the trailing edge of a splitter plate. Therefore, to reduce the uncertainties of estimating initial turbulence kinetic energy and dissipation energy rate, and to make the computational approach applicable in the entire flow field, a method for predicting recirculating flow field is needed. For the application to supersonic combustor development, the interaction between the supersonic and subsonic flow fields becomes important. The downstream pressure effects which are neglected in the present parabolic flow computer program should also be considered.

CONCLUDING REMARKS

The three-dimensional parabolic flow computer program SHIP has been evaluated both analytically and numerically. To achieve the efficiency in both computer storage and computing time, many mathematical and physical simplifications have been introduced into the program. A numerical evaluation has been performed for several two- and three-dimensional turbulent, reacting and nonreacting flow fields. Good predictions are generally obtained from the program when the simplifications are justified.

For the application to supersonic combustor development, the present computer program is mainly limited mathematically by the parabolic flow assumption and physically by the equilibrium chemistry simplification. Continuing studies to remove these limitations are needed. Provided that recirculation (if present) and downstream pressure effects can be properly modeled or separately calculated and the reaction model can be improved, the present parabolic flow computer program is capable of predicting complicated flow fields in combustors. Thus, the present program is potentially valuable for supersonic combustor development and experimentation.

APPENDIX
DERIVATION OF THE DIFFERENCE EQUATION

The derivation of the general form of the finite-difference equation (2) from the differential equation (1) is outlined in this Appendix for completeness. Details can be found in many publications of Spalding's group (for example, refs. 1, 4, 9).

Equation (1) can be transformed into a finite-difference equation by integrating it over the control volume surrounding an arbitrary mode P shown in figure 22 by dotted lines. W, E, S, N are, respectively, the neighboring nodes of P in the west, east, south, and north directions. The points, w, e, s, n are the midpoints of the lines PW, PE, PS and PN, respectively. In the z-direction, ϕ varies in a stepwise manner; this makes the finite-difference scheme fully implicit. For the calculation of the z-direction convection and of source terms, the variation of ϕ in the xy plane is also taken to be stepwise. That is, in the xy plane, the value of ϕ is assumed to remain uniform and equal to ϕ_p over the dotted rectangle (fig. 22) surrounding the point P and to change sharply to ϕ_W, ϕ_E, ϕ_S or ϕ_N outside the rectangle. For the cross-stream convection from the xz and yz faces of the control volume, the value of ϕ convected is taken to be the arithmetic mean of the ϕ values on either side of that face. For diffusion across the xz and yz faces of the control volume, ϕ varies linearly between two neighboring grid points.

When the integrations of various terms in equation (1) are expressed in the manner described above, the following form of difference equations is obtained,

$$F_D\phi_p - F_U\phi_{p,U} + [L_e^x (\phi_E + \phi_p) - L_w^x (\phi_W + \phi_p)] - [T_e^x (\phi_E - \phi_p) - T_w^x (\phi_p - \phi_W)]$$

$$+ [L_n^y (\phi_N + \phi_p) - L_s^y (\phi_S + \phi_p)] - [T_n^y (\phi_N - \phi_p) - T_s^y (\phi_p - \phi_S)]$$

$$= S_U + S_p \phi_p \qquad \text{(A1)}$$

where

$$F_U = (\Delta x)(\Delta y)(\rho w)_{p,U}/\Delta z$$

$$L^x = (\Delta y)(\rho u)_U/2$$

$$L^y = (\Delta x)(\rho v)_U/2$$

$$F_D = F_U - 2L_e^x + 2L_w^x - 2L_n^y + 2L_s^y \qquad \text{(A2)}$$

$$T^x = P_\phi (\Delta y)/\delta x$$

$$T^y = P_\phi (\Delta x)/\delta y$$

$$S_U + S_p\phi_p = S_\phi (\Delta x)(\Delta y)$$

Rearranging the terms in eq. (A1) yields equation (2),

$$\phi_p = A_N\phi_N + A_S\phi_S + A_E\phi_E + A_W\phi_W + B \tag{A2}$$

where

$$A_N = (T_n^y - L_n^y)/A_p$$

$$A_S = (T_s^y + L_s^y)/A_p$$

$$A_E = (T_e^x - L_e^x)/A_p \tag{A3}$$

$$A_W = (T_w^x + L_w^x)/A_p$$

$$B = (F_U\phi_{p,U} + S_U)/A_p$$

with

$$A_p = (T_n^y - L_n^y) + (T_s^y + L_s^y) + (T_e^x - L_e^x) + (T_w^x + L_w^x) + F_U - S_p \tag{A4}$$

When the lateral convection (denoted by the symbol L) is large, some of the coefficients A_N, A_S, A_E and A_W can become negative, a modification by the "hybrid" scheme is used (ref. 17). The modification consists of replacing all the T's by $\tilde{T}$'s defined by

$$\tilde{T} = \frac{1}{2}\{T + |L| + |T - |L||\} \tag{A5}$$

Hence, $\tilde{T}$ is always positive.

REFERENCES

1. Patankar, S. V.; and Spalding, D. B.: Numerical Prediction of Three-Dimensional Flow. Report EF/TN/A/46, Mech. Eng. Dept., Imperial College, 1972.
2. Baker, A. J.: Finite-Element Solution Theory for Three-Dimensional Boundary-Layer Flows, Comp. Meth. Appl. Mech. Eng., vol. 4, pp. 367-386, 1974.
3. Briley, W. R.; McDonald, H.; and Gibeling, H. J.: Solution of the Multidimensional Compressible Navier-Stokes Equations by a Generalized Implicit Method. R75-911363-15, United Technologies Research Center 1976.
4. Patankar, S. V.; and Spalding, D. B.: A Calculation Procedure for Heat, Mass, and Momentum Transfer in Three-Dimensional Parabolic Flows. Int. J. Heat Mass Transfer, vol. 15, 1972, pp. 1787-1806.
5. Curr, R. M.; Sharma, D.; and Tatchell, D. G.: Numerical Predictions of Some Three-Dimensional Boundary Layers in Ducts. Comp. Meth. in Appl. Mech. Eng., vol. 1, 1972, pp. 143-158.
6. Patankar, S. V.; Pratap, V. S.; and Spalding, D. B.: Prediction of Turbulent Flow in Curved Pipes. J. Fluid Mech., vol. 67, 1975, pp. 583-595.
7. Serag-Eldin, M. A.; and Spalding, D. B.: Prediction of the Flow and Combustion Processes in a Three-Dimensional Combustion Chamber. Proceedings of the 3rd International Symposium on Airbreathing Engines. K. H. Dietmar and G. Winterfeld, ed., DGLR (Munich, Germany), 1976, pp. 489-514.

8. Markatos, N. C.; Spalding, D. B.; and Tatchell, D. G.: Combustion of Hydrogen Injected into a Supersonic Airstream (The SHIP Computer Program). NASA CR-2802, 1977.

9. Dyer, D. F.; Maples, G.; and Spalding, D. B.: Combustion of Hydrogen Injected into a Supersonic Airstream (A Guide to the HISS Computer Program). NASA CR-2655, 1976.

10. Spalding, D. B.: A Novel Finite Difference Formulation for Differential Expressions Involving Both First and Second Derivatives. Int. J. Numerical Meth. Eng., vol. 4, 1972, pp. 551-559.

11. Caretto, L. S.; Gosman, A. D.; Patankar, S. V.; and Spalding, D. B.: Two Calculation Procedures for Steady, Three-Dimensional Flows with Recirculation. Proc. of 3rd Int. Conf. on Numerical Methods in Fluid Mechanics, Springer Verlag, 1972, pp. 60-68.

12. Spalding, D. B.: Numerical Computation of Steady Boundary Layers - A Survey. Computational Methods and Problems in Aeronautical Fluid Dynamics. B. L. Hewitt, ed., Academic Press (New York), 1976, pp. 466-491.

13. Patankar, S. V.: Numerical Prediction of Three-Dimensional Flows. Studies in Convection. B. E. Lauder, ed., vol. 1, Academic Press (New York), 1975, pp. 1-78.

14. Launder, B. E.; and Spalding, D. B.: The Numerical Computation of Turbulent Flows. Comp. Meth. in Appl. Mech. Eng., vol. 3, 1974, pp. 269-289.

15. Runchal, A. K.: Convergence and Accuracy of Three Finite Difference Schemes for a Two-Dimensional Conduction and Convection Problem. Int. J. Numerical Meth. Eng., vol. 4, 1972, pp. 541-550.

16. Coles, D. E.; and Hirst, E. A., eds.: Proceedings of Computation of Turbulent Boundary Layer - 1968, AFOSR-IFP-STANFORD CONFERENCE. vol. II Stanford University, 1968.

17. Launder, B. E.; and Spalding, D. B.: Lectures in Mathematical Models of Turbulence. Academic Press, 1972.

18. Brown, G. L.; and Roshko, A.: On Density Effects and Large Structure in Turbulent Mixing Layers. J. Fluid Mech., vol. 64, 1974, pp. 775-816.

19. Launder, B. E.; Morse, A.; Rodi, W.; and Spalding, D. B.: Prediction of Free Shear Flows, A Comparison of the Performance of Six Turbulence Models. Free Turbulent Shear Flows. vol. 1, NASA SP-321, 1972.

20. Schlicting, H.: Boundary Layer Theory. Fourth edition; McGraw Hill, 1960.

21. Salas, M. D.: Shock Fitting Method for Complicated Two-Dimensional Supersonic Flow. AIAA (Journal), vol. 14, no. 5, 1976, pp. 583-588.

22. Rogers, R. C.: Mixing of Hydrogen Injected from Multiple Injectors Normal to a Supersonic Airstream. NASA TN D-6476, 1971.

23. Burrows, M. C.; and Kurkov, A. P.: Supersonic Combustion of Hydrogen in a Vitiated Air Stream Using Stepped-Wall Injection. AIAA Paper No. 71-721. AIAA/SAE 7th Propulsion Joint Specialist Conference, Salt Lake City, Utah, June 14-18, 1971.

24. Burrows, M. C.; and Kurkov, A. P.: An Analytical and Experimental Study of Supersonic Combustion of Hydrogen in a Vitiated Airstream. AIAA (Journal), vol. 11, 1973, pp. 1217-1218. (Also, NASA TM X-2828, 1973.)

25. Kurkov, A. P.; and Gaugler, R. E.: Diffusive Ignition and Combustion in a Wall Jet. NASA TM X-71496, 1974.

26. Spalding, D. B.: Turbulent Modeling: Solved and Unsolved Problems. Turbulent Mixing in Non-reactive and Reactive Flow, ed. by S. N. B. Murthy, Plenum Press, 1975, pp. 85-130.

TABLE I

The Appropriate Exchange Coefficients and Source Terms for Variable ϕ

ϕ	Γ_ϕ	S_ϕ
1	0	0
u	μ_{eff}	$-\frac{\partial p}{\partial x} + \frac{\partial}{\partial x}\left[\frac{\mu_{eff}}{3}\left(\frac{\partial u}{\partial x} - 2\frac{\partial v}{\partial y}\right)\right] + \frac{\partial}{\partial y}\left[\mu_{eff}\frac{\partial v}{\partial x}\right]$
v	μ_{eff}	$-\frac{\partial p}{\partial y} + \frac{\partial}{\partial y}\left[\frac{\mu_{eff}}{3}\left(\frac{\partial v}{\partial y} - 2\frac{\partial u}{\partial x}\right)\right] + \frac{\partial}{\partial x}\left[\mu_{eff}\frac{\partial u}{\partial y}\right]$
w	μ_{eff}	$-\frac{\partial p}{\partial z}$
H	$\frac{\mu_{eff}}{Pr_{eff,h}}$	$\frac{\partial}{\partial x}\left[\frac{\mu_{eff}}{Pr_{eff,h}}(Pr_{eff,h}-1)\frac{\partial}{\partial x}\left(\frac{u^2+v^2+w^2}{2}\right)\right]$ $+\frac{\partial}{\partial y}\left[\frac{\mu_{eff}}{Pr_{eff,h}}(Pr_{eff,h}-1)\frac{\partial}{\partial y}\left(\frac{u^2+v^2+w^2}{2}\right)\right]$ $+\mu_{eff}\left[\left(\frac{\partial u}{\partial x}\right)^2 + \left(\frac{\partial v}{\partial y}\right)^2 + 2\frac{\partial u}{\partial y}\frac{\partial v}{\partial x}\right]$
f	$\frac{\mu_{eff}}{Pr_{eff,f}}$	0

TABLE I (Concluded)

ϕ	Γ_ϕ	S_ϕ
k	$\frac{\mu_{eff}}{Pr_{eff,k}}$	$\mu_t \left\{ 2 \left[\left(\frac{\partial u}{\partial x}\right)^2 + \left(\frac{\partial v}{\partial y}\right)^2 \right] + \left(\frac{\partial w}{\partial x}\right)^2 + \left(\frac{\partial w}{\partial y}\right)^2 + \left(\frac{\partial u}{\partial y} + \frac{\partial v}{\partial x}\right)^2 \right\} - \rho\varepsilon$
ε	$\frac{\mu_{eff}}{Pr_{eff,\varepsilon}}$	$C_1 \frac{\varepsilon}{k} \mu_t \left\{ 2 \left[\left(\frac{\partial u}{\partial x}\right)^2 + \left(\frac{\partial v}{\partial y}\right)^2 \right] + \left(\frac{\partial w}{\partial x}\right)^2 + \left(\frac{\partial w}{\partial y}\right)^2 + \left(\frac{\partial u}{\partial y} + \frac{\partial v}{\partial x}\right)^2 \right\} - C_2 \frac{\rho\varepsilon^2}{k}$

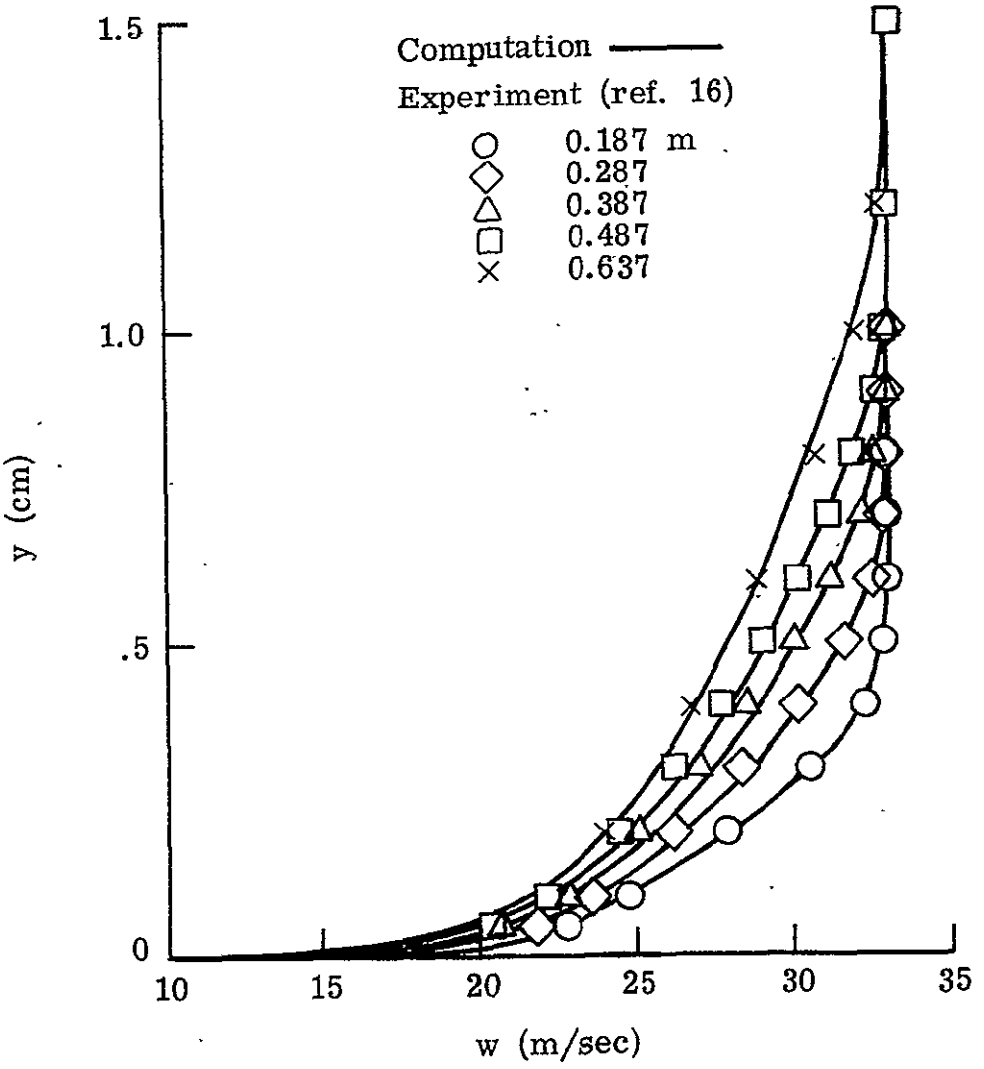

Figure 1.- Turbulent boundary layer velocity profiles.

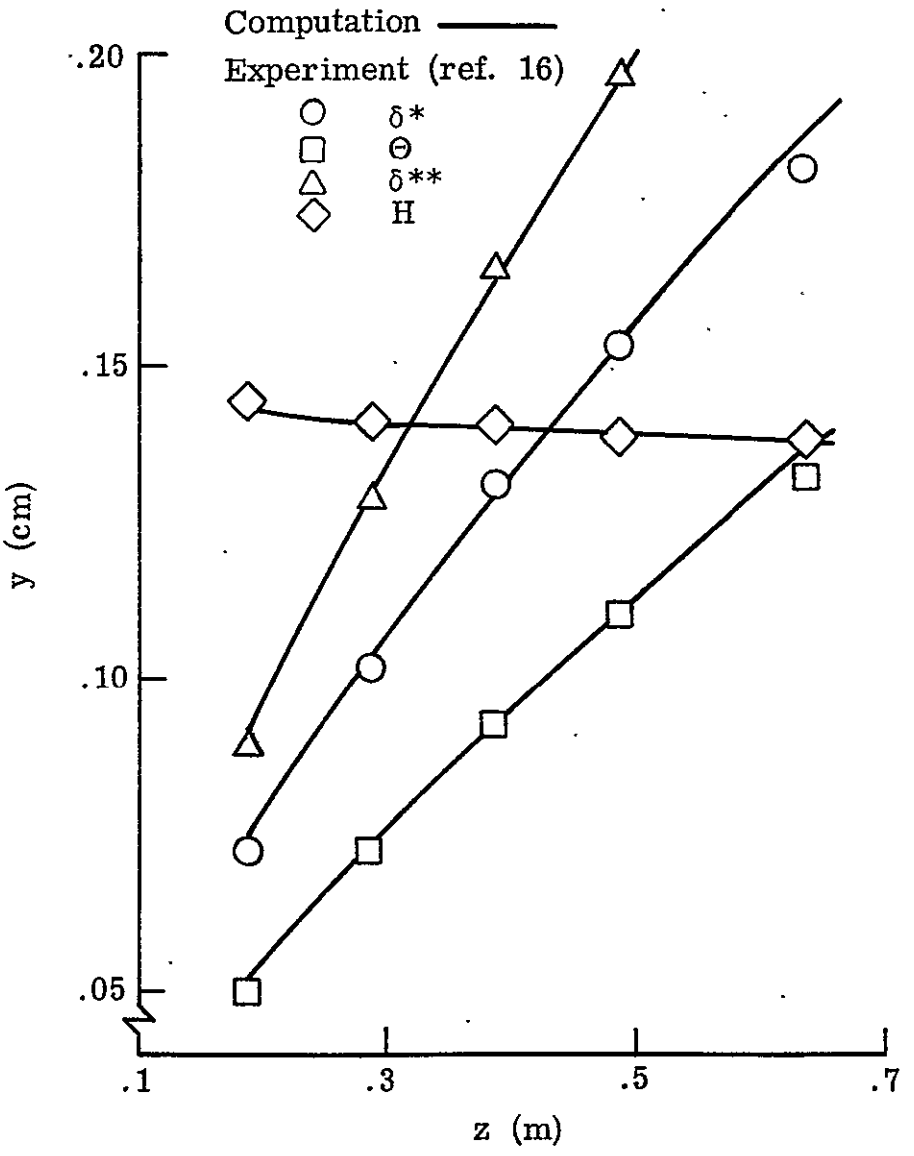

Figure 2.- Integral parameters of a turbulent boundary layer.

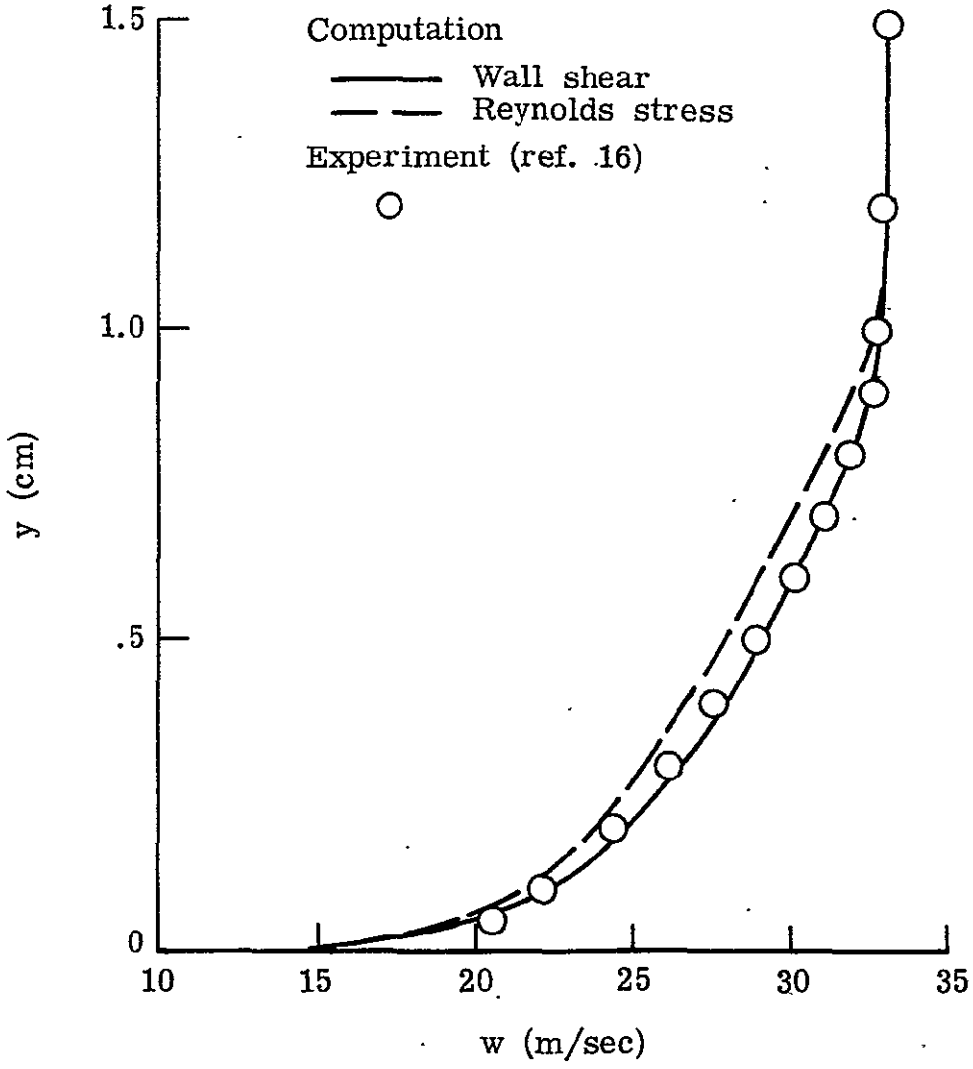

Figure 3.- A typical comparison of velocity profiles at z = 0.487 m based on two different shear stresses in the wall function.

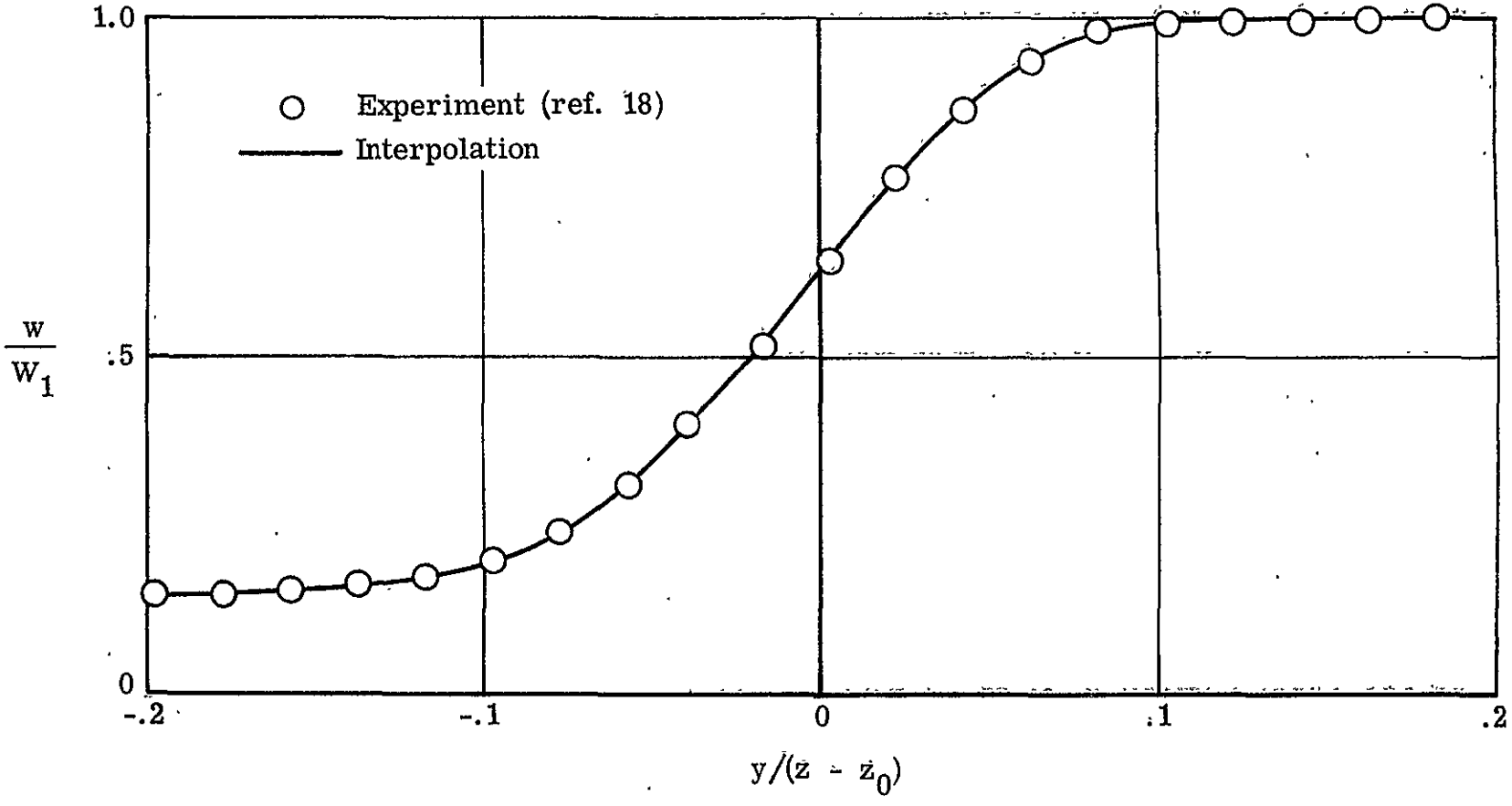

Figure 4.- Initial velocity profile of an Air-Air mixing layer.
($W_1/W_2 = 7$, $z_o = -6.35 \times 10^{-3}$ m, $z = 0.0254$ m)

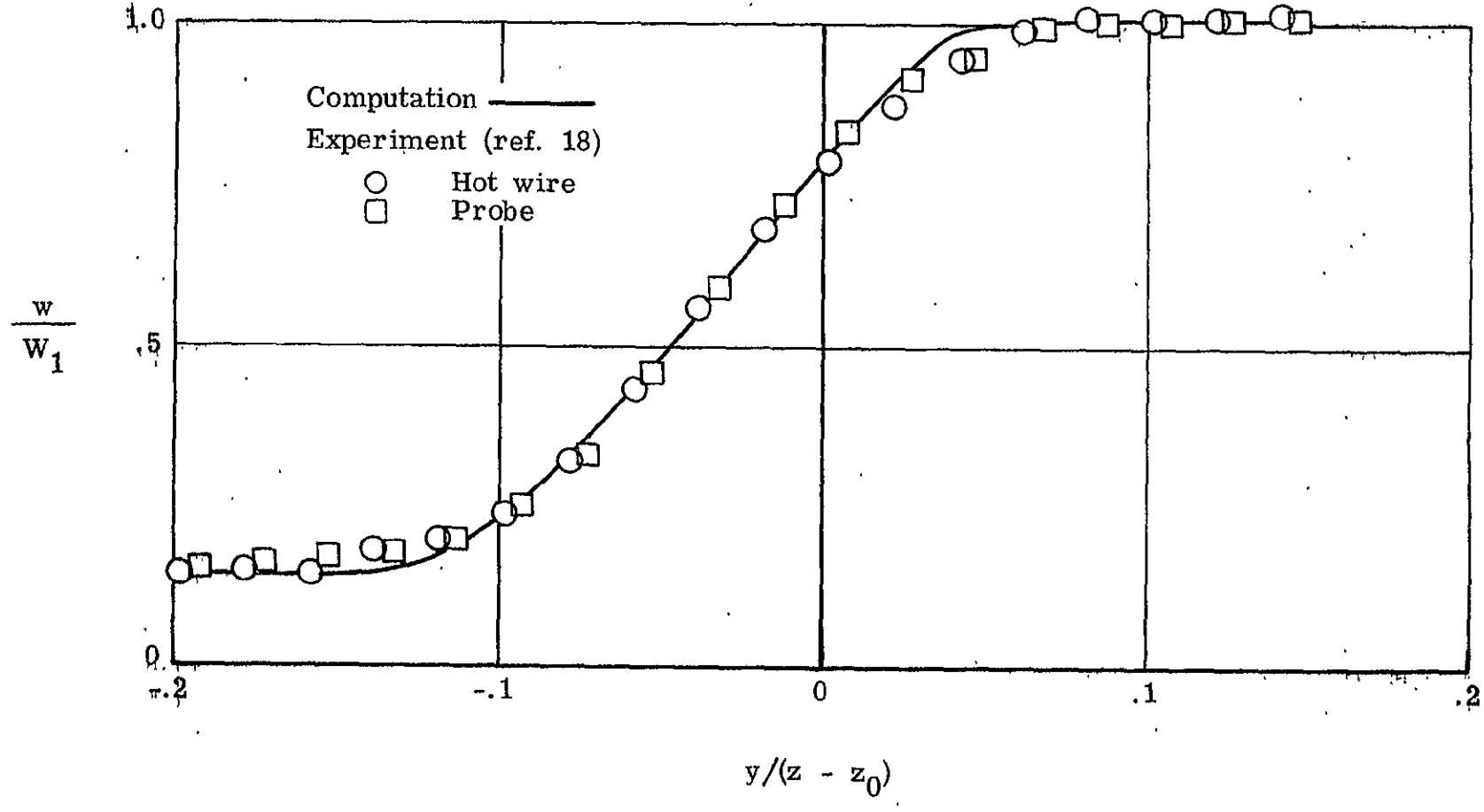

(a) z = 0.0508 m.

Figure 5.- Velocity profile of an Air-Air mixing layer.
($W_1/W_2 = 7$, $z_0 = -6.35 \times 10^{-3}$ m)

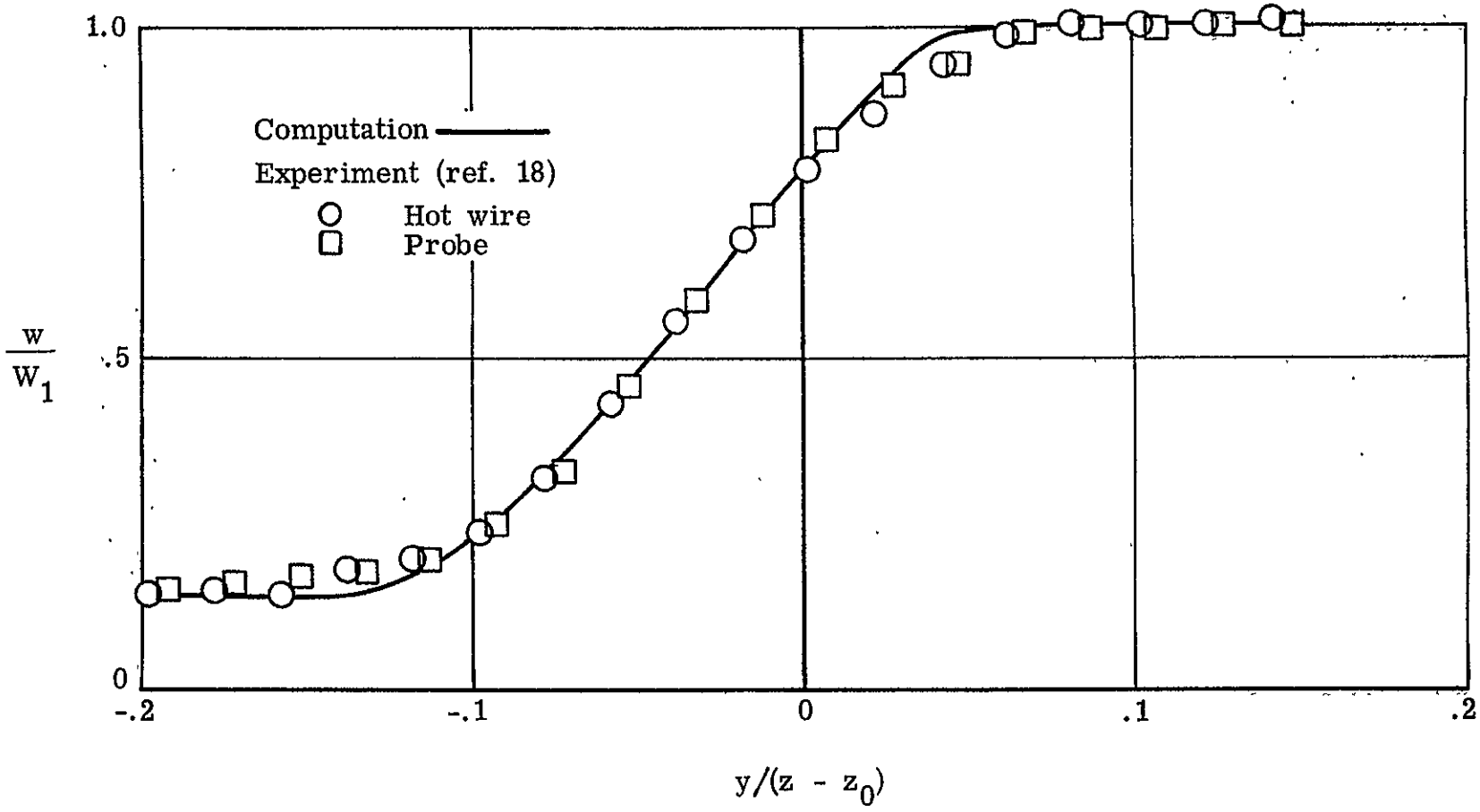

(b) z = 0.0635 m.

Figure 5.- Continued.

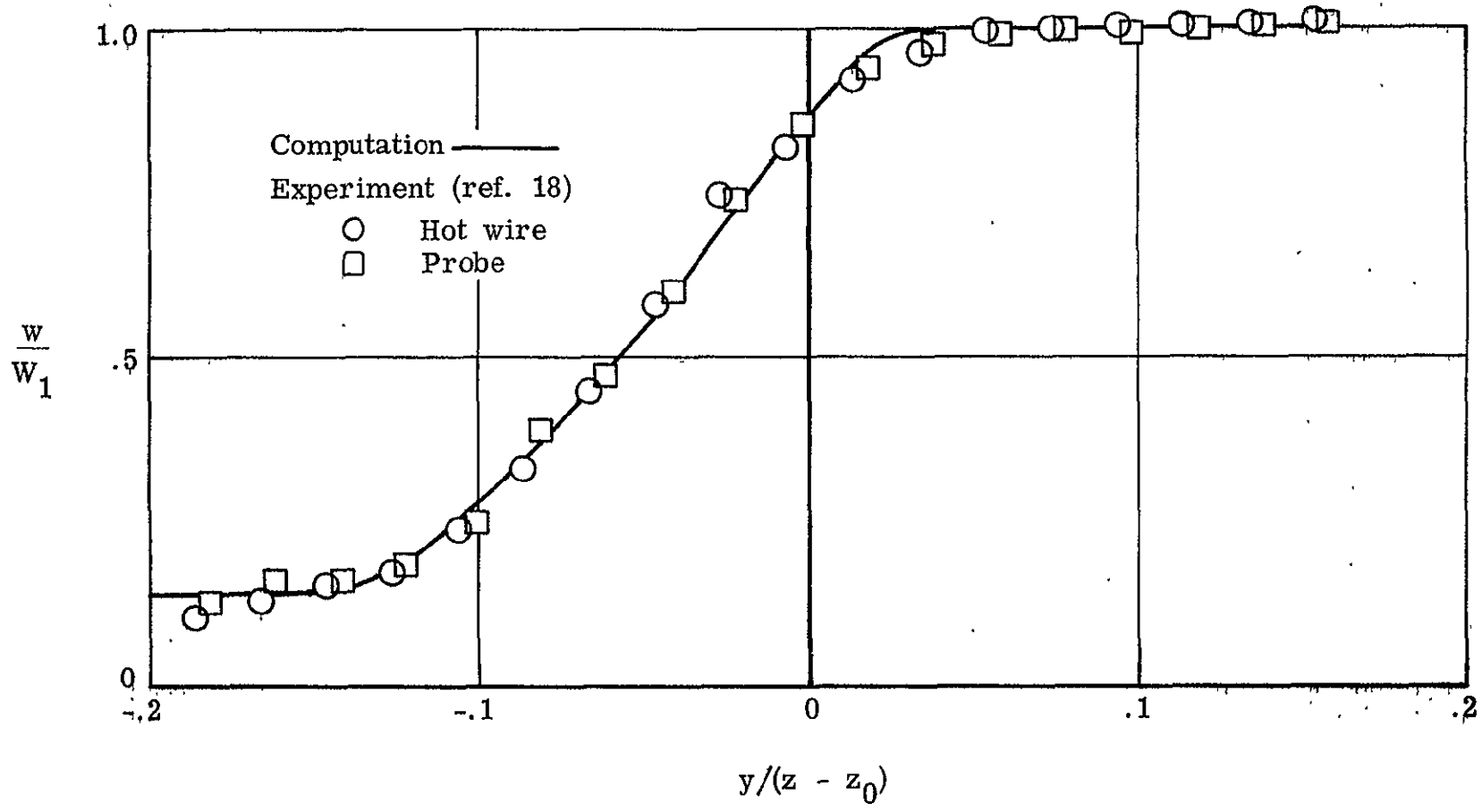

(c) z = 0.0762 m.

Figure 5.- Continued.

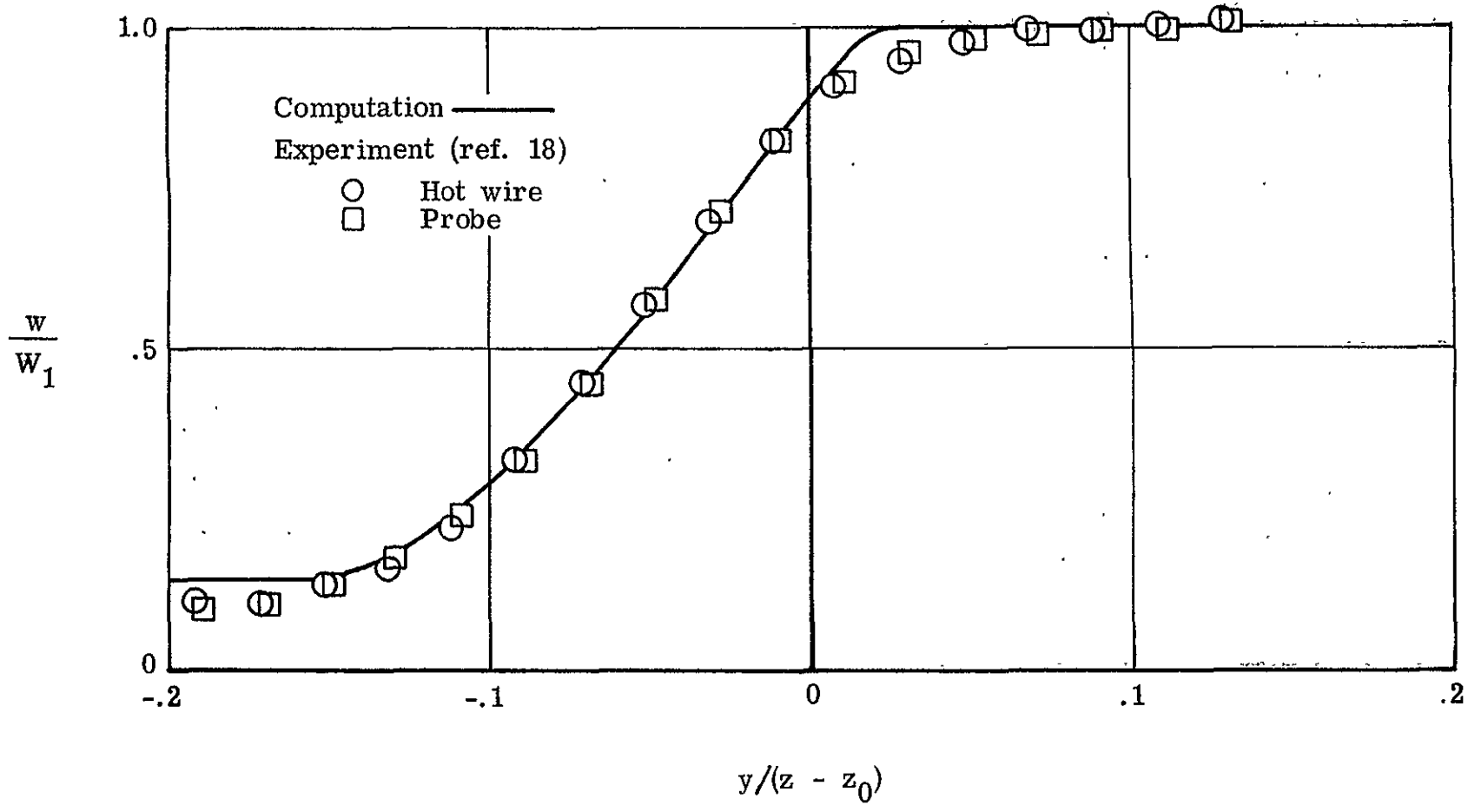

(d) z = 0.0889 m.

Figure 5.- Concluded.

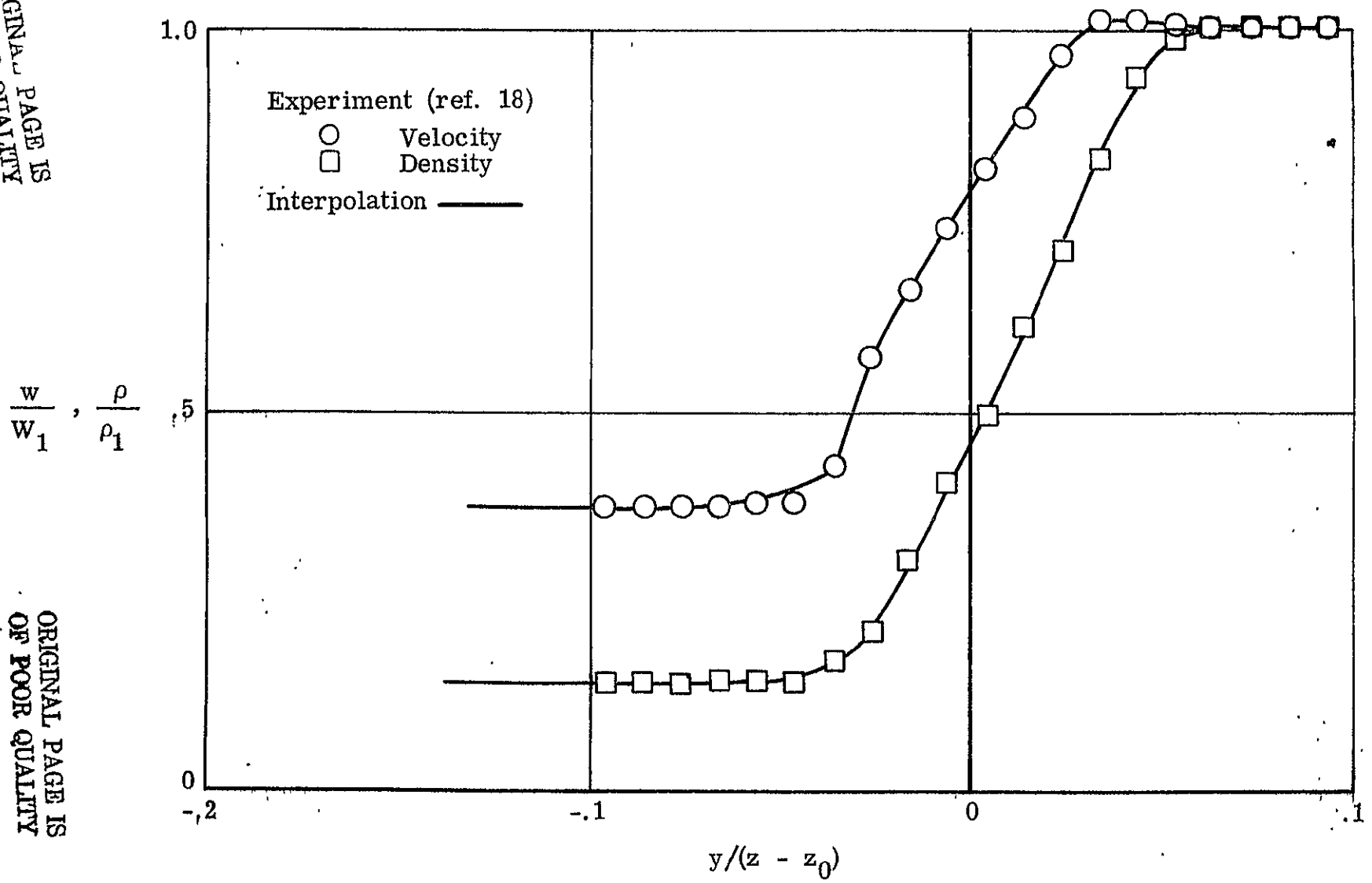

Figure 6.- Initial velocity and density profiles of a N_2-He mixing layer.
($W_1/W_2 = 7^{1/2}$, $\rho_1/\rho_2 = 7$, $z_o = -0.0254$ m, $z = 0.0254$ m)

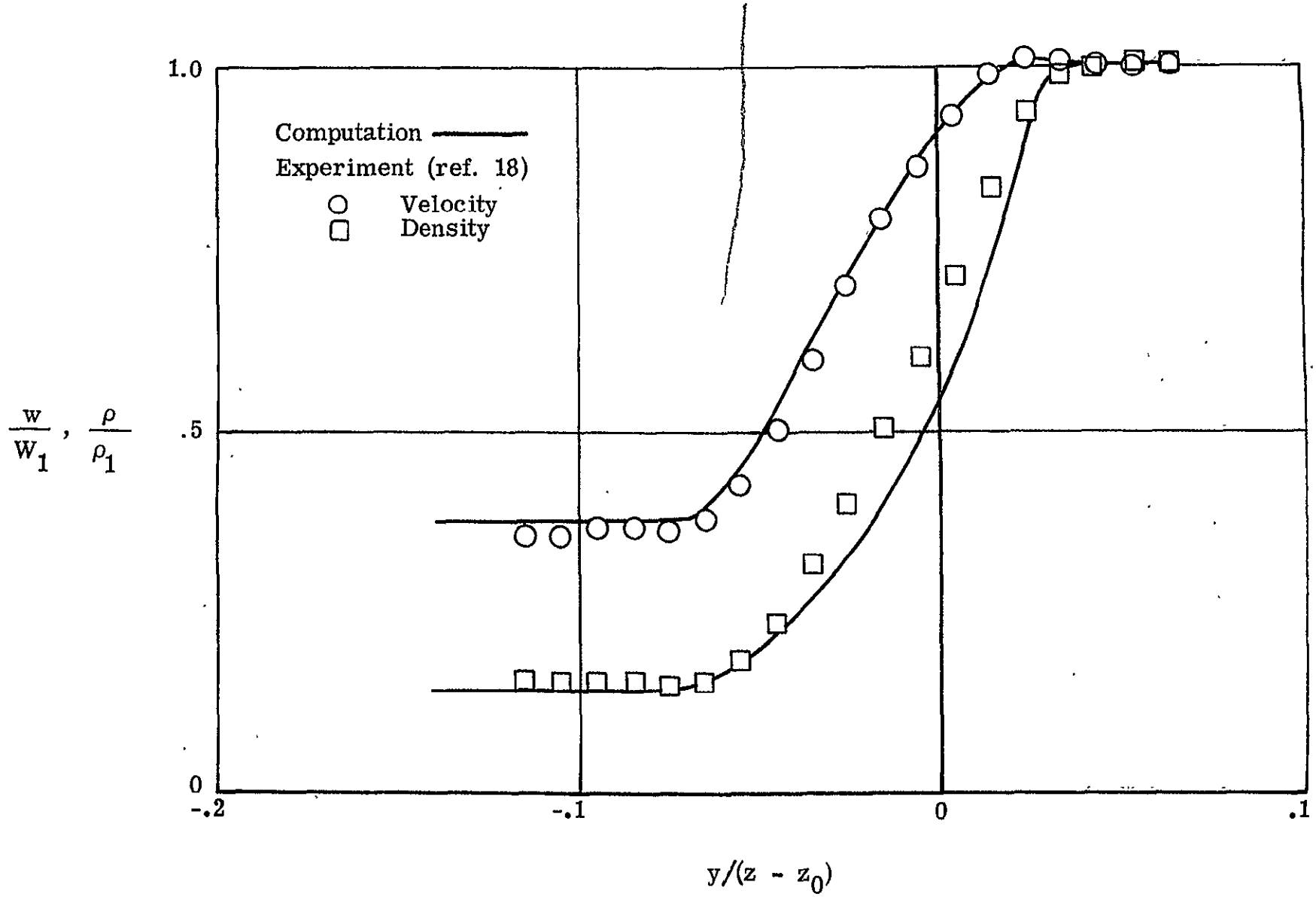

(a) z = 0.0508 m.

Figure 7.- Velocity and density profiles of a N_2-He mixing layer.
($W_1/W_2 = 7^{\frac{1}{2}}$, $\rho_1/\rho_2 = 7$, $z_o = -0.0254$ m)

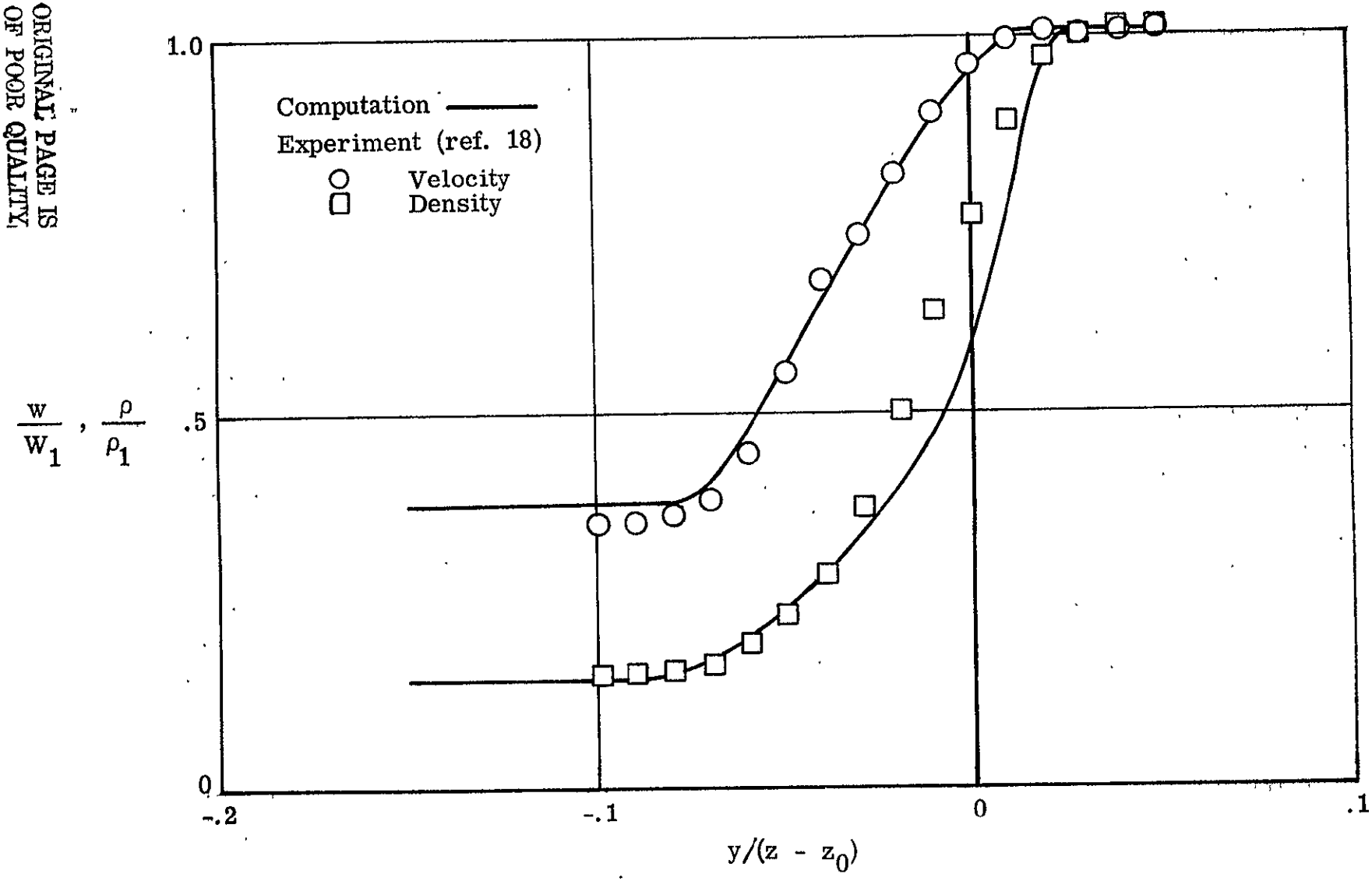

(b) z = 0.0762 m.

Figure 7.- Continued.

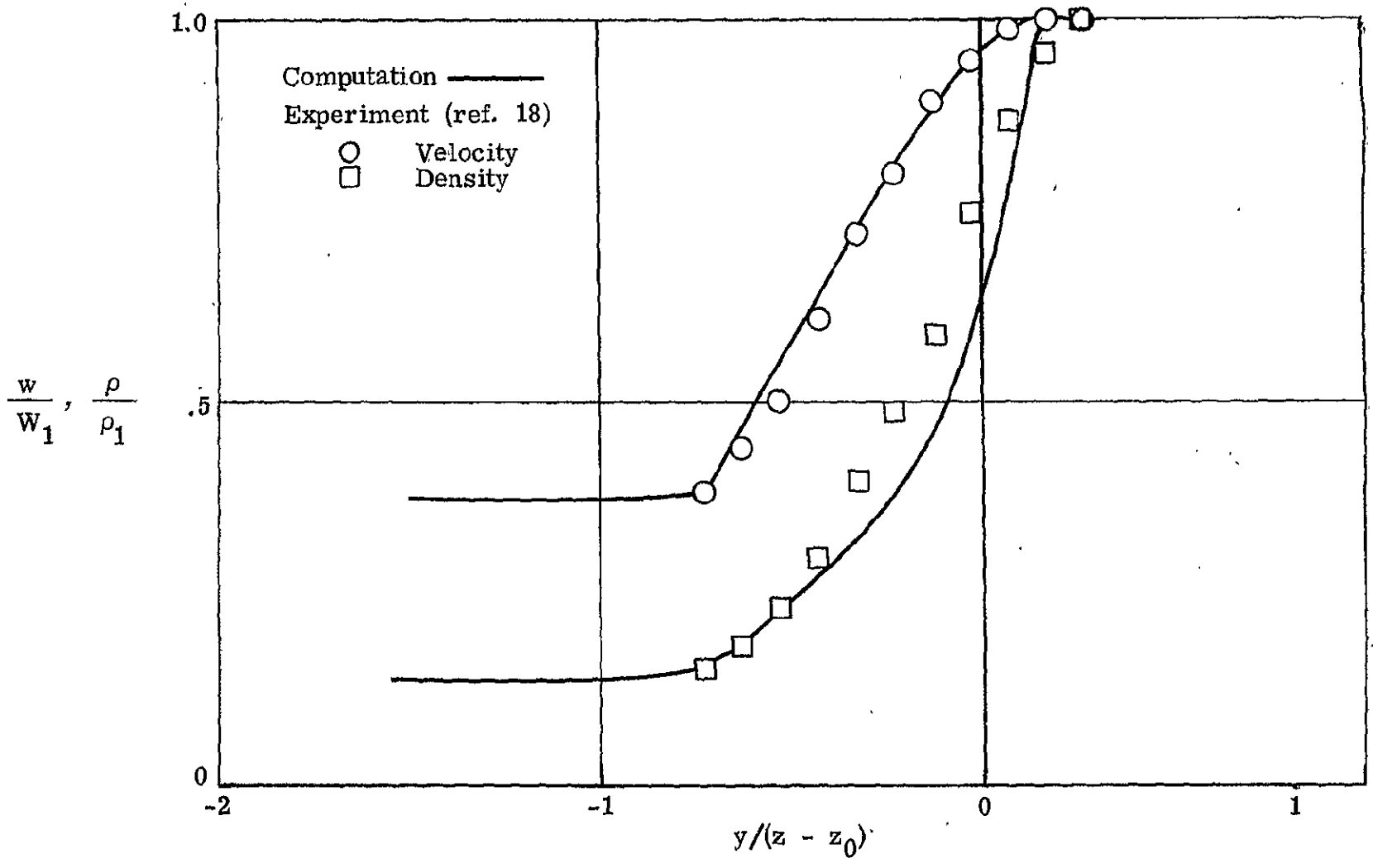

(c) z = 0.1016 m

Figure 7.- Concluded.

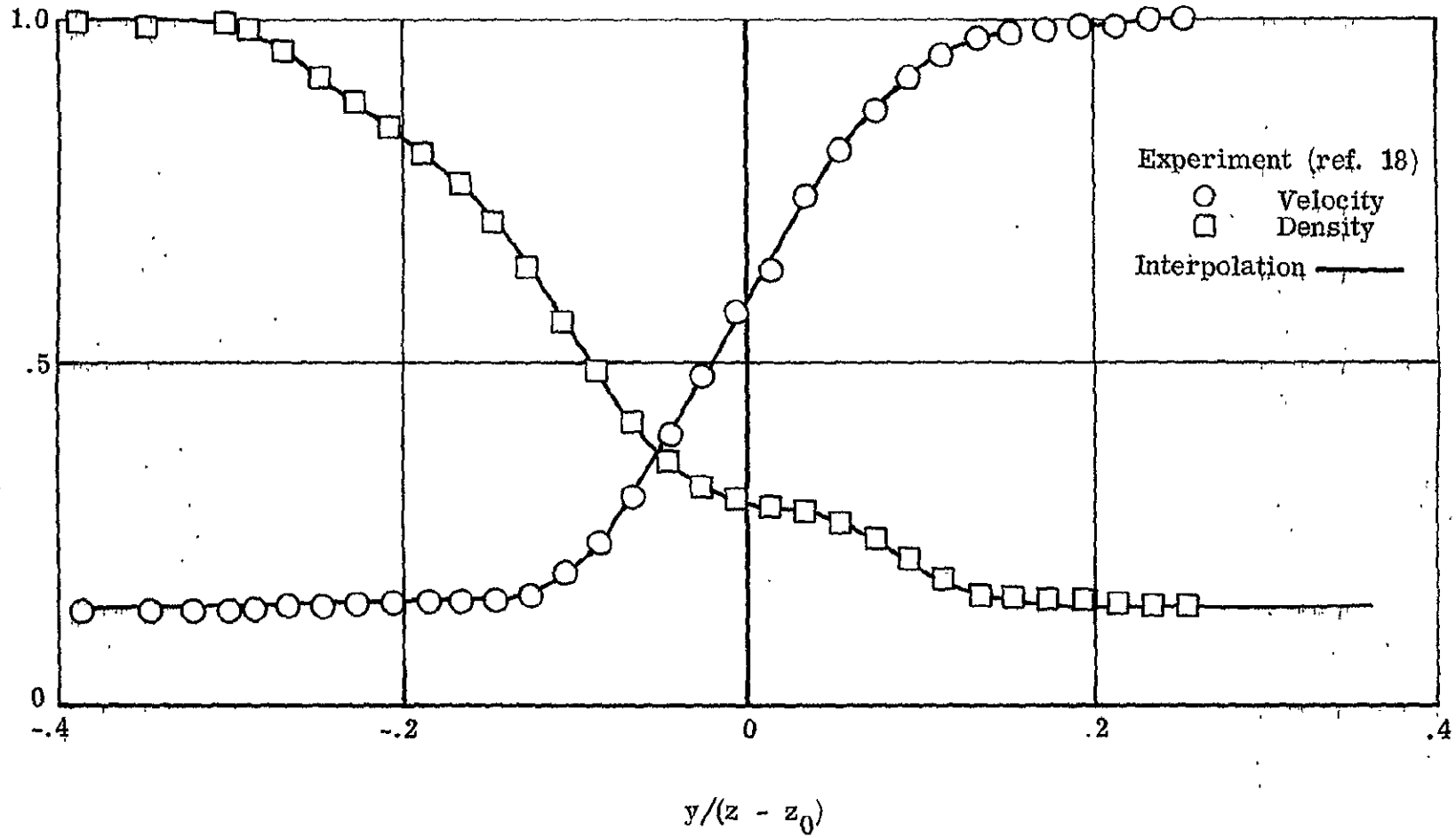

Figure 8.- Initial velocity and density profiles of a N_2-He mixing layer. ($W_1/W_2 = 7$, $\rho_1/\rho_2 = 1/7$, $z_o = 1.27 \times 10^{-3}$ m, $z = 0.0254$ m)

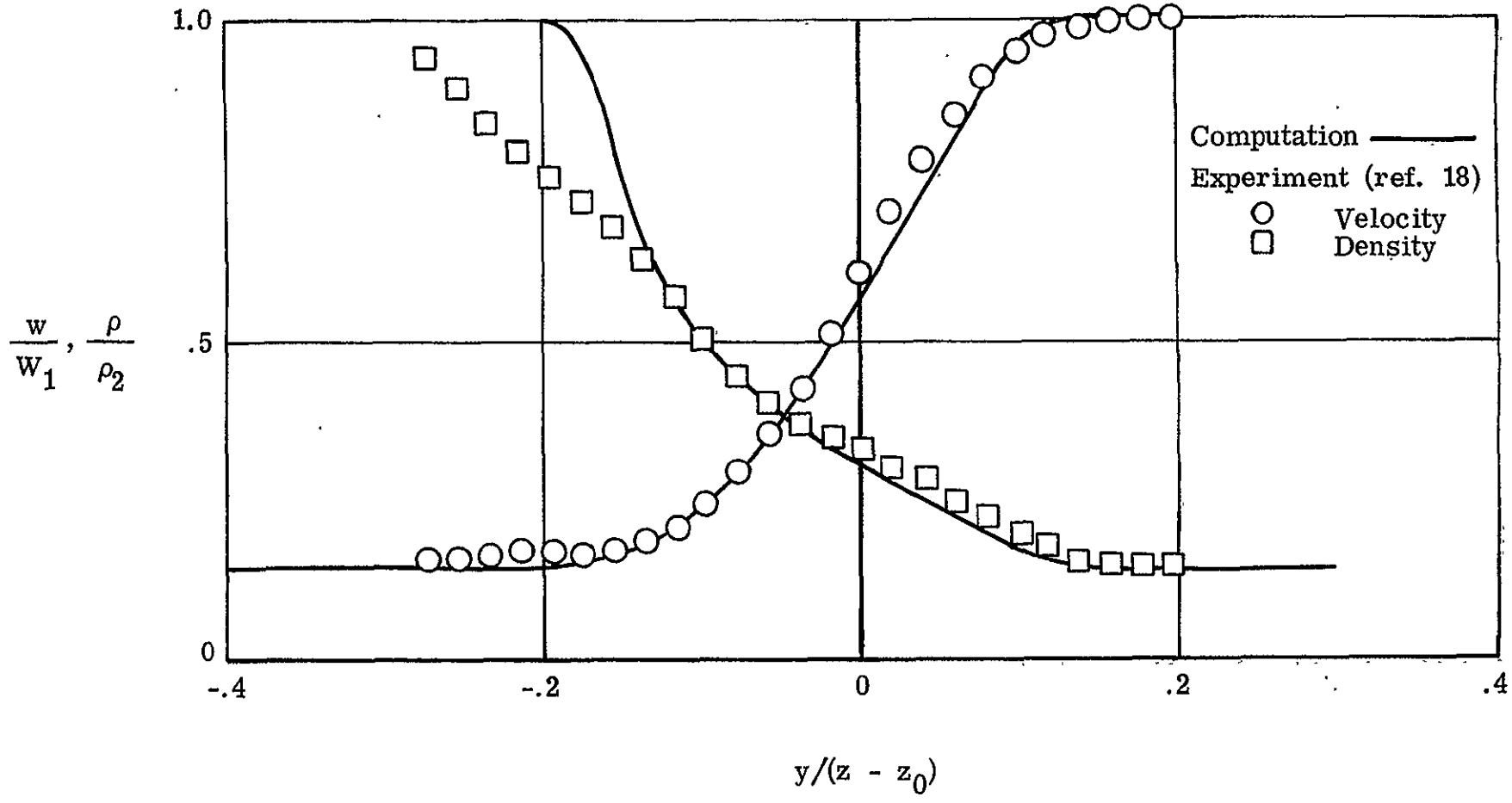

(a) z = 0.0508 m.

Figure 9.- Velocity and density profiles of a N_2-He mixing layer.
($W_1/W_2 = 7$, $\rho_1/\rho_2 = 1/7$, $z_o = 1.27 \times 10^{-3}$ m)

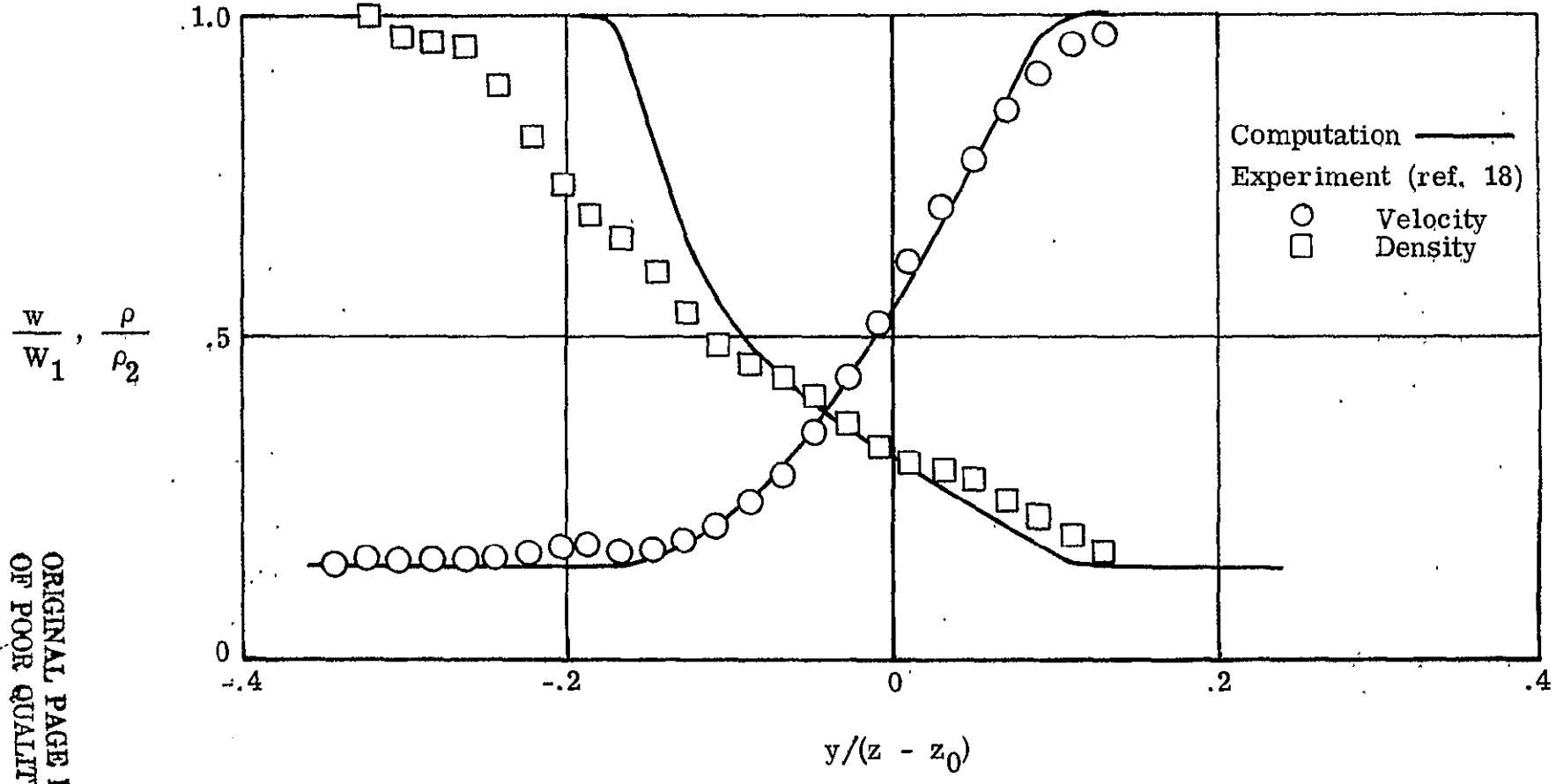

(b) z = 0.0635 m.

Figure 9.- Continued

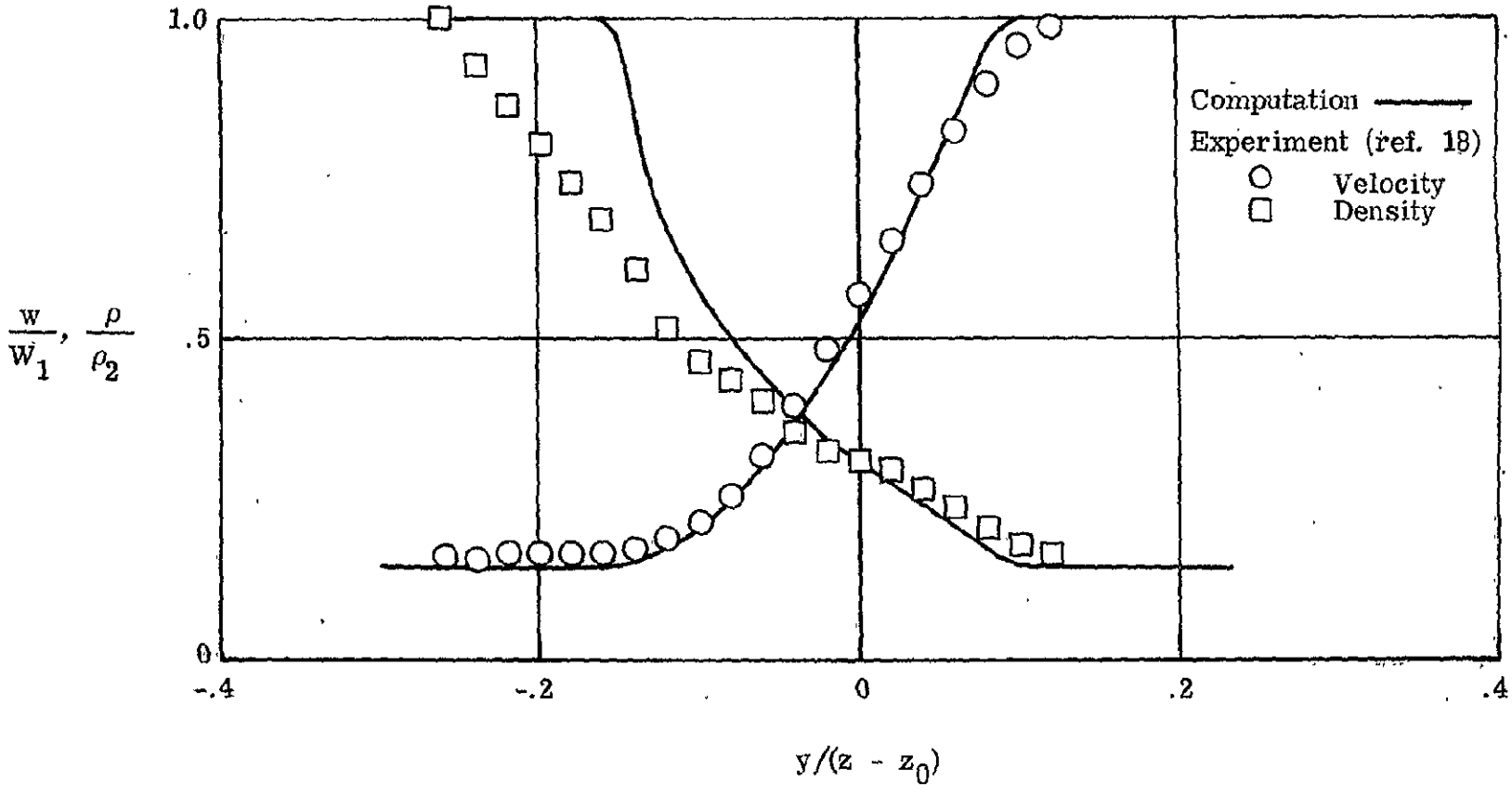

(c) z = 0.0762 m

Figure 9.- Continued.

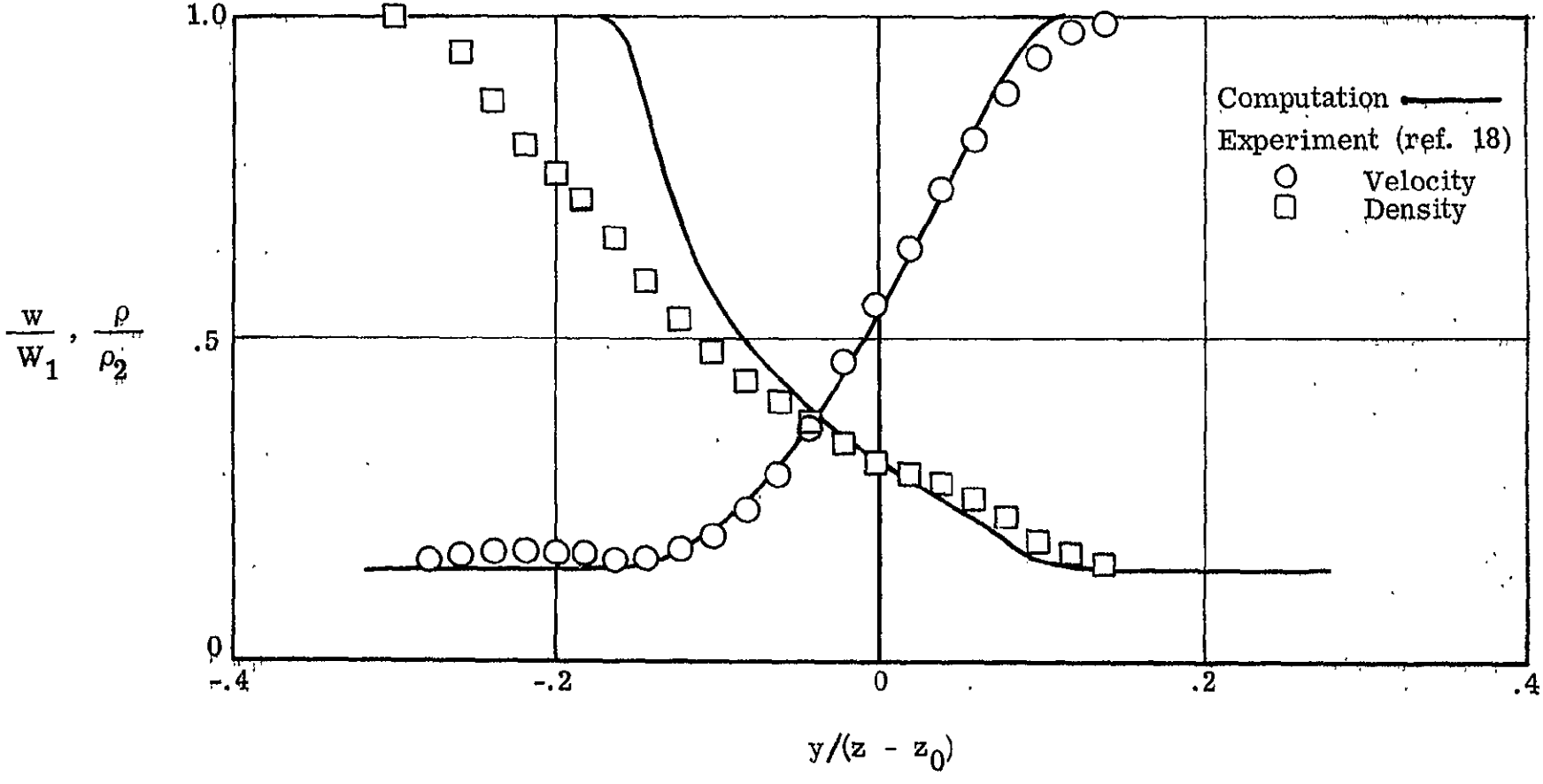

(d) z = 0.0889 m.

Figure 9.- Concluded.

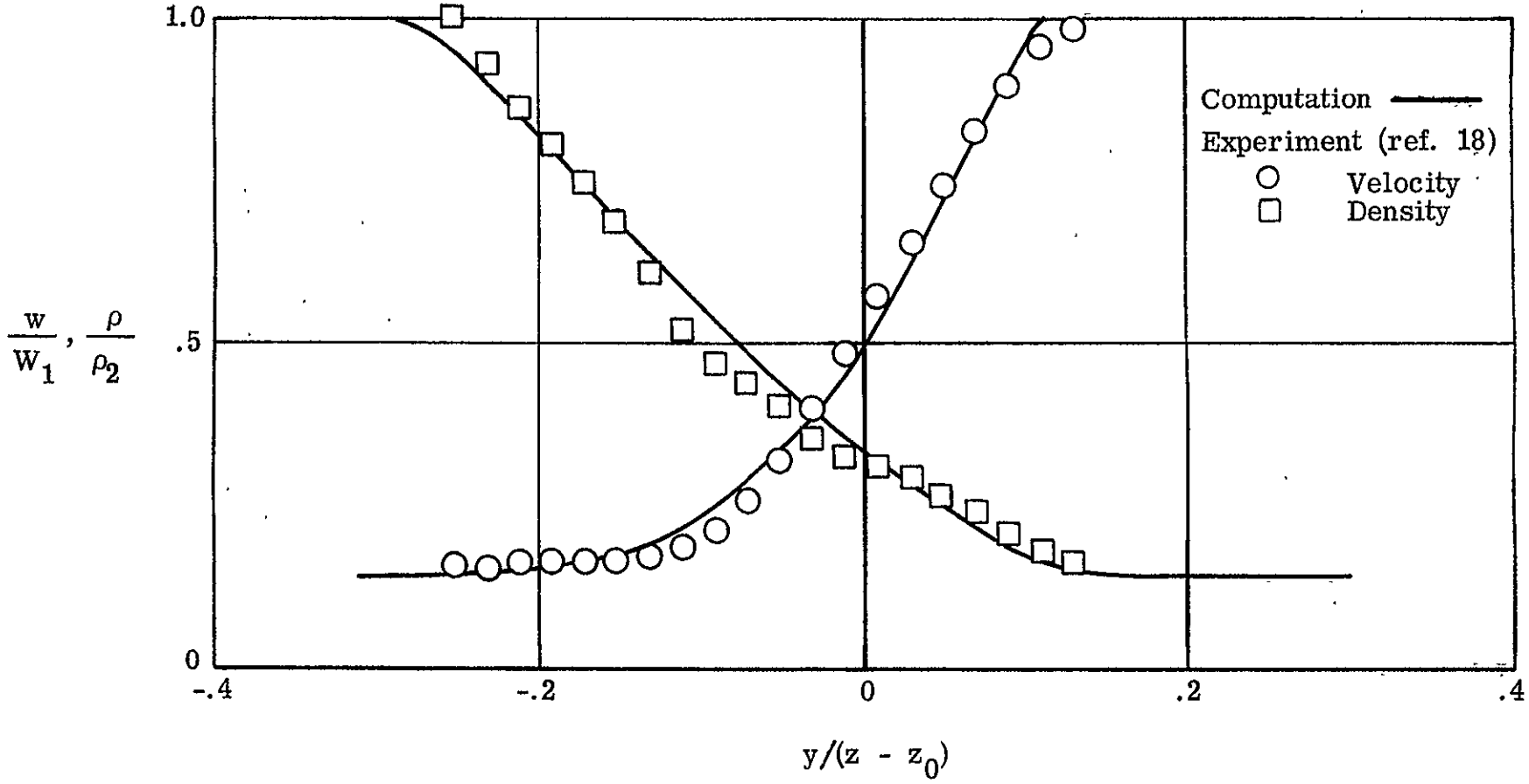

Figure 10.- Typical velocity and density profiles of a N_2-He mixing layer with a density-dependent mixing length.
($W_1/W_2 = 7$, $\rho_1/\rho_2 = 1/7$, $z_o = 1.27 \times 10^{-3}$ m, $z = 0.0889$ m)

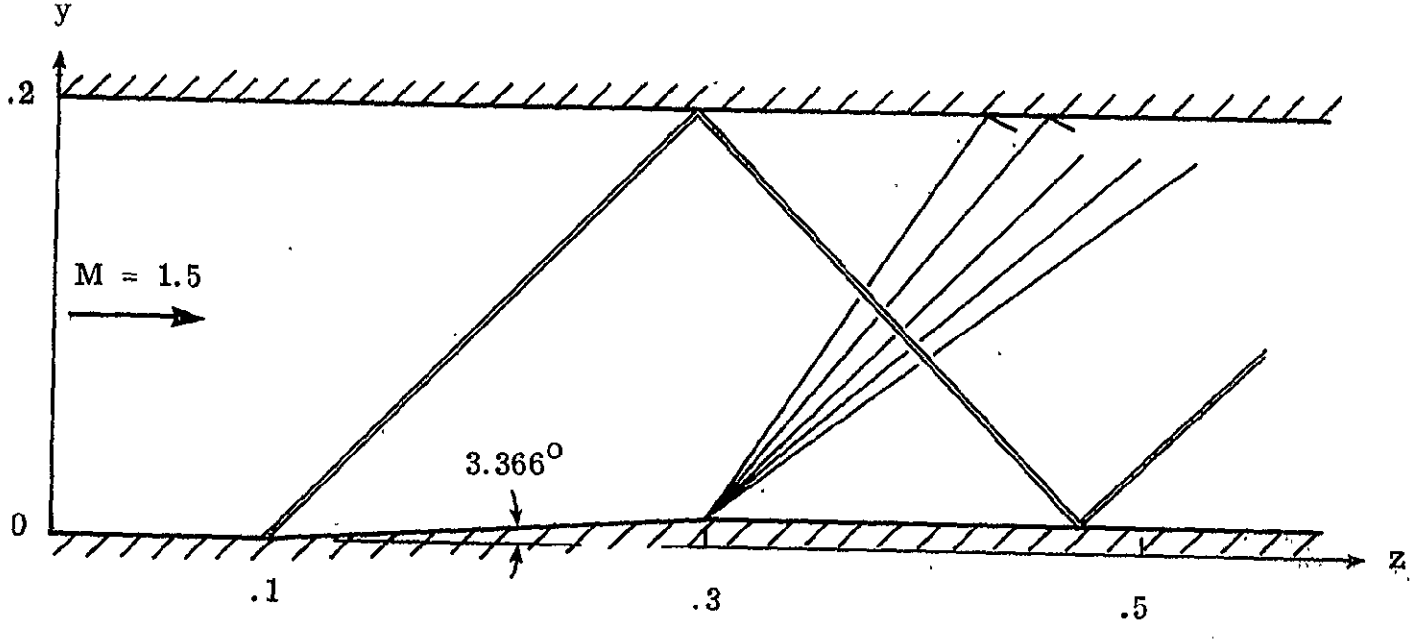

Figure 11.- The geometry and wave pattern of a two-dimensional supersonic channel flow.

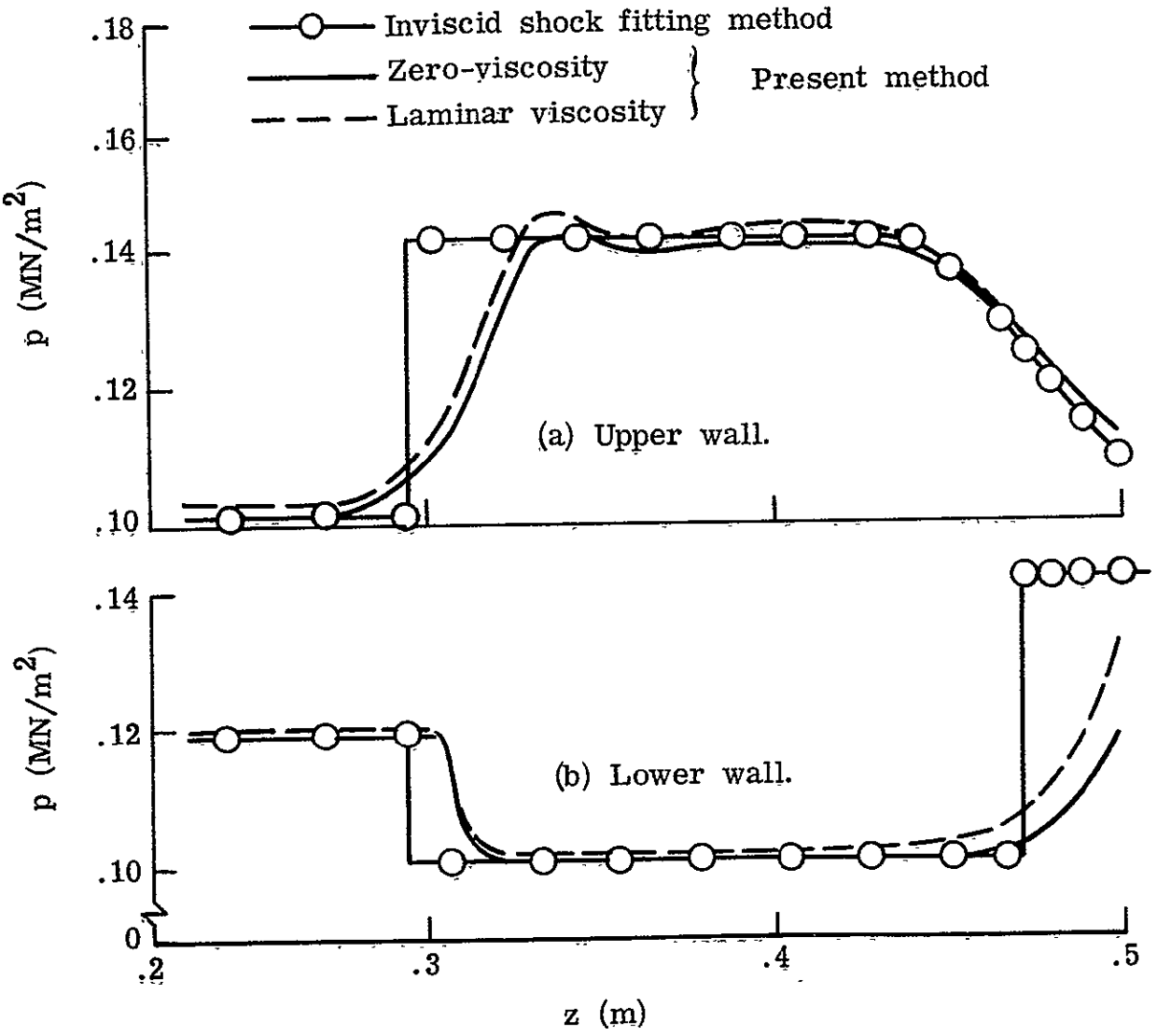

Figure 12.- Comparison of wall pressures.

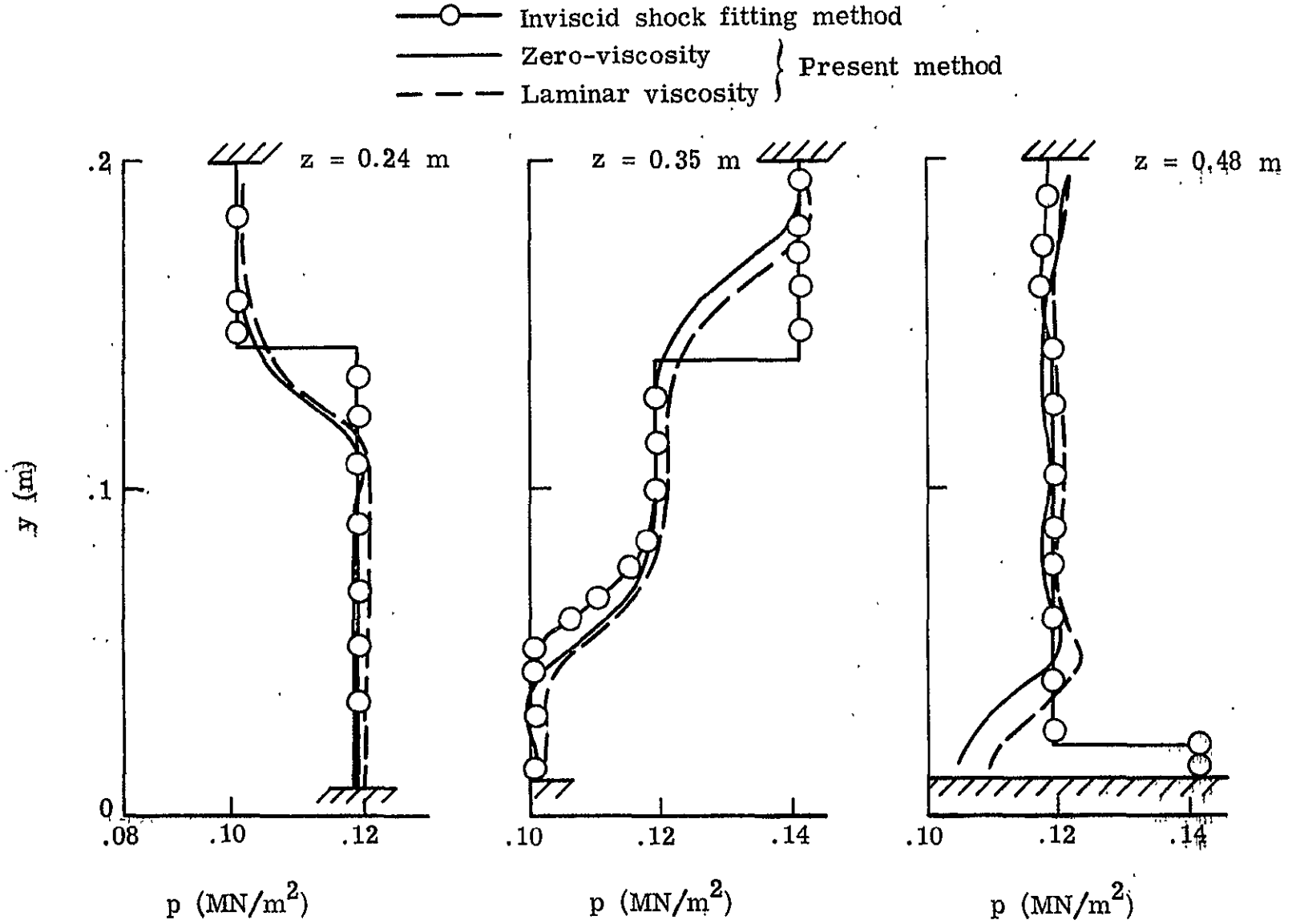

Figure 13.- Comparison of pressure profiles across the channel.

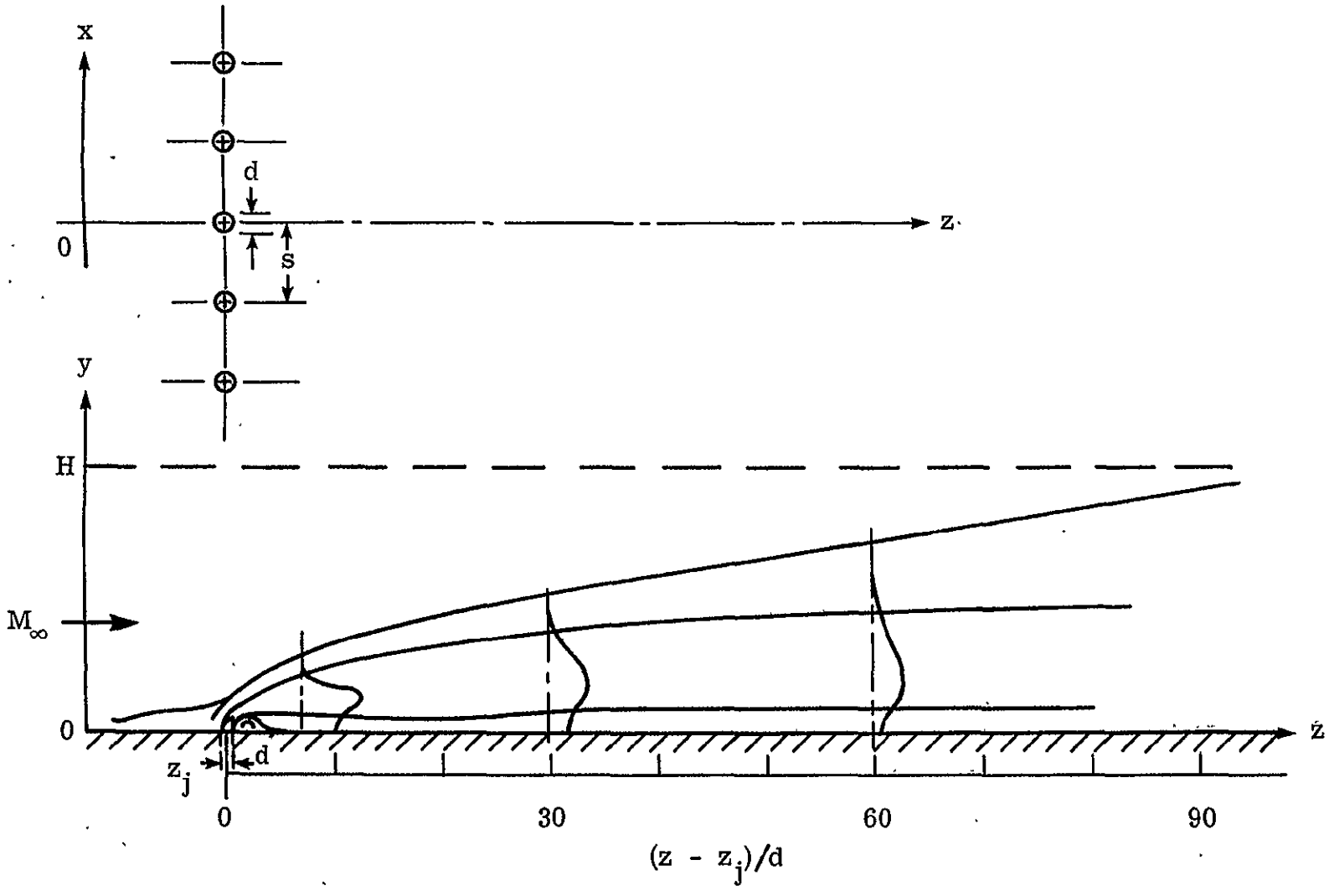

Figure 14.- Flow field and injector arrangement of a three-dimensional normal injection problem.

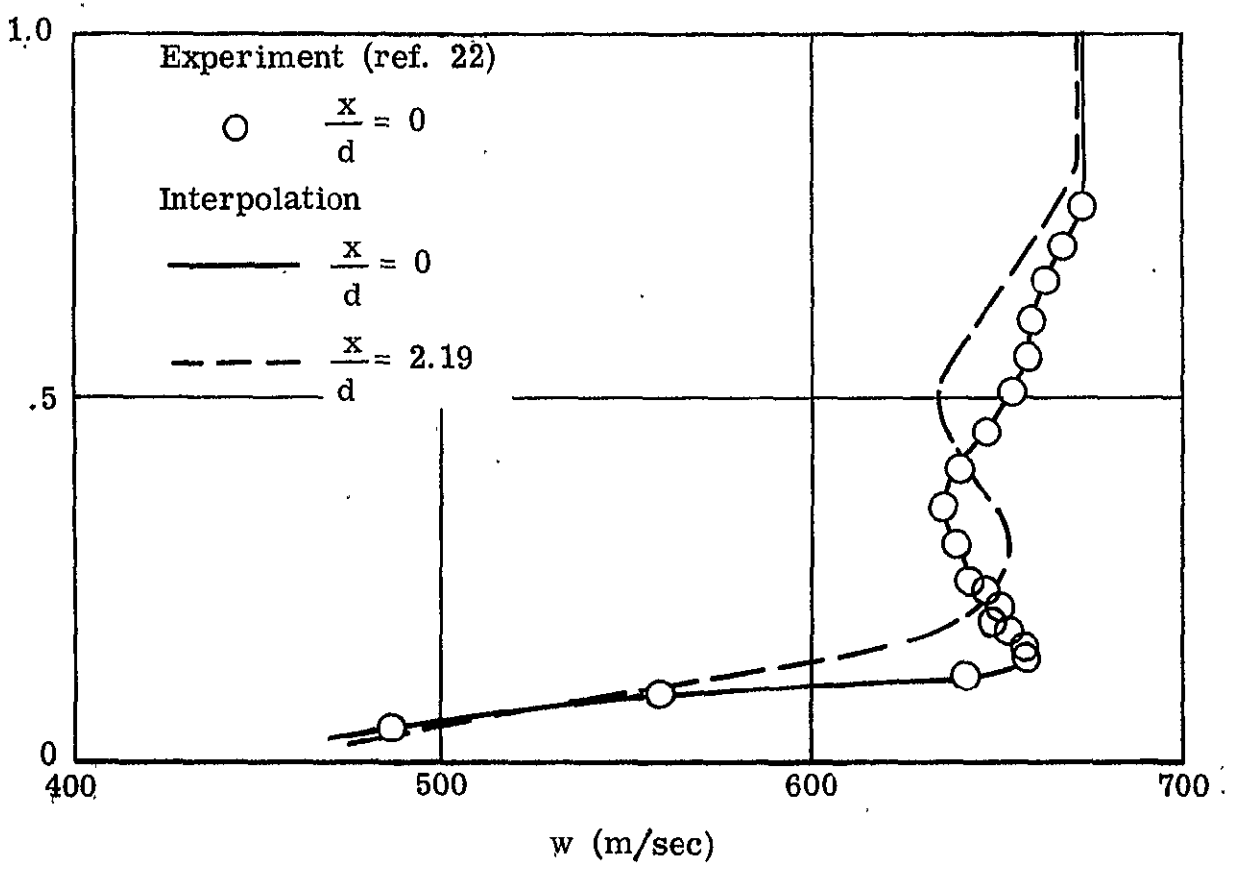

(a) Velocity.

Figure 15.- Initial profiles and experimental data.
($s/d = 6.25$, $(z-z_j)/d = 30$)

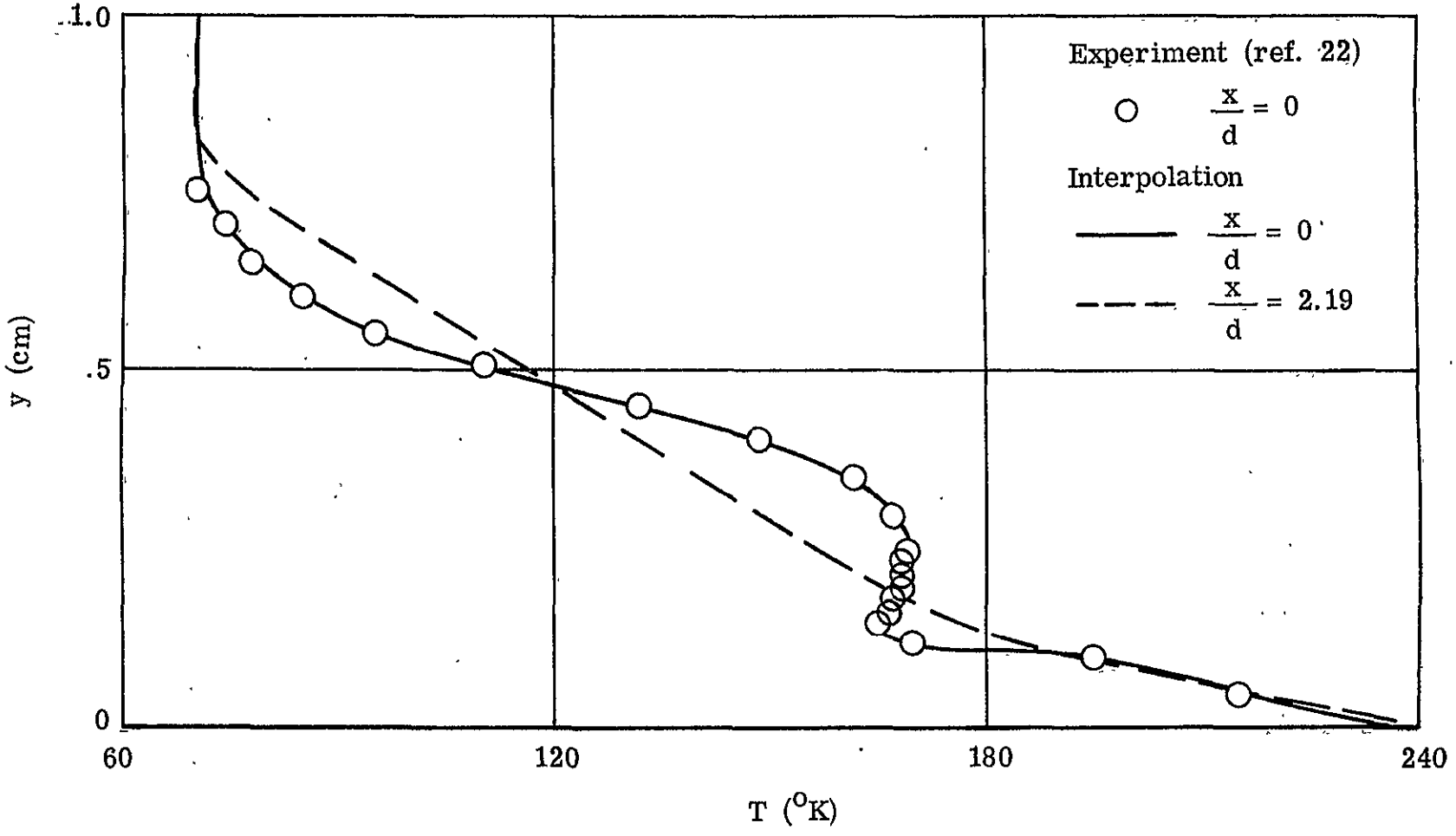

(b) Temperature.

Figure 15.- Continued.

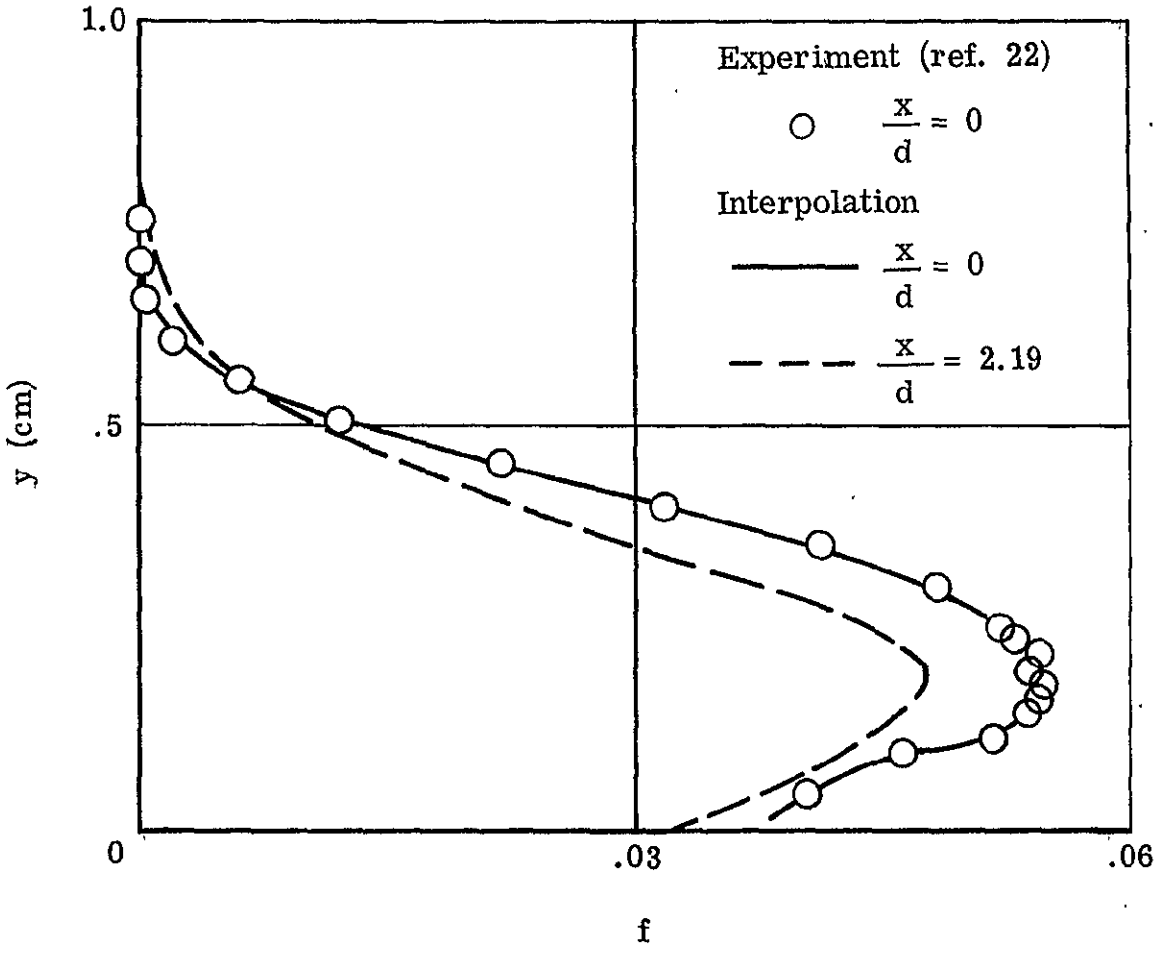

(c) Hydrogen concentration.

Figure 15.- Continued.

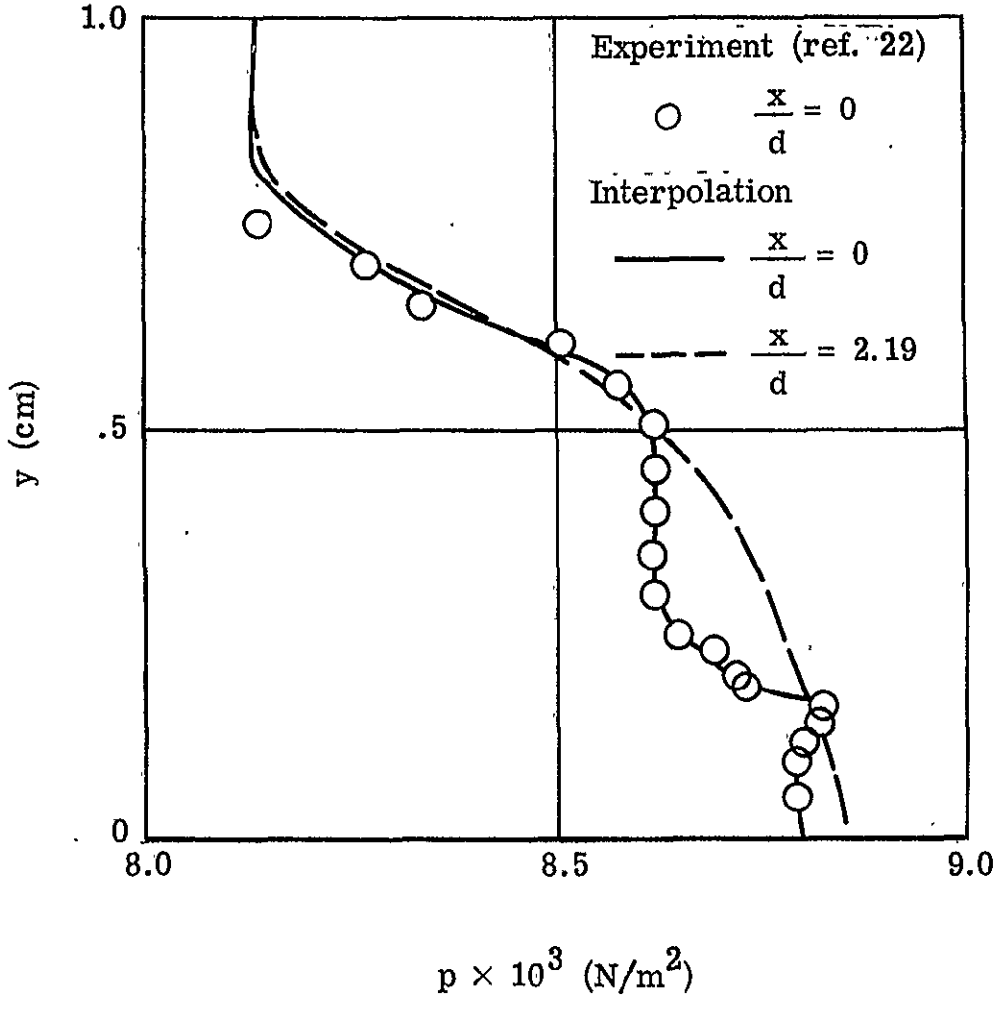

(d) Pressure.

Figure 15.- Concluded.

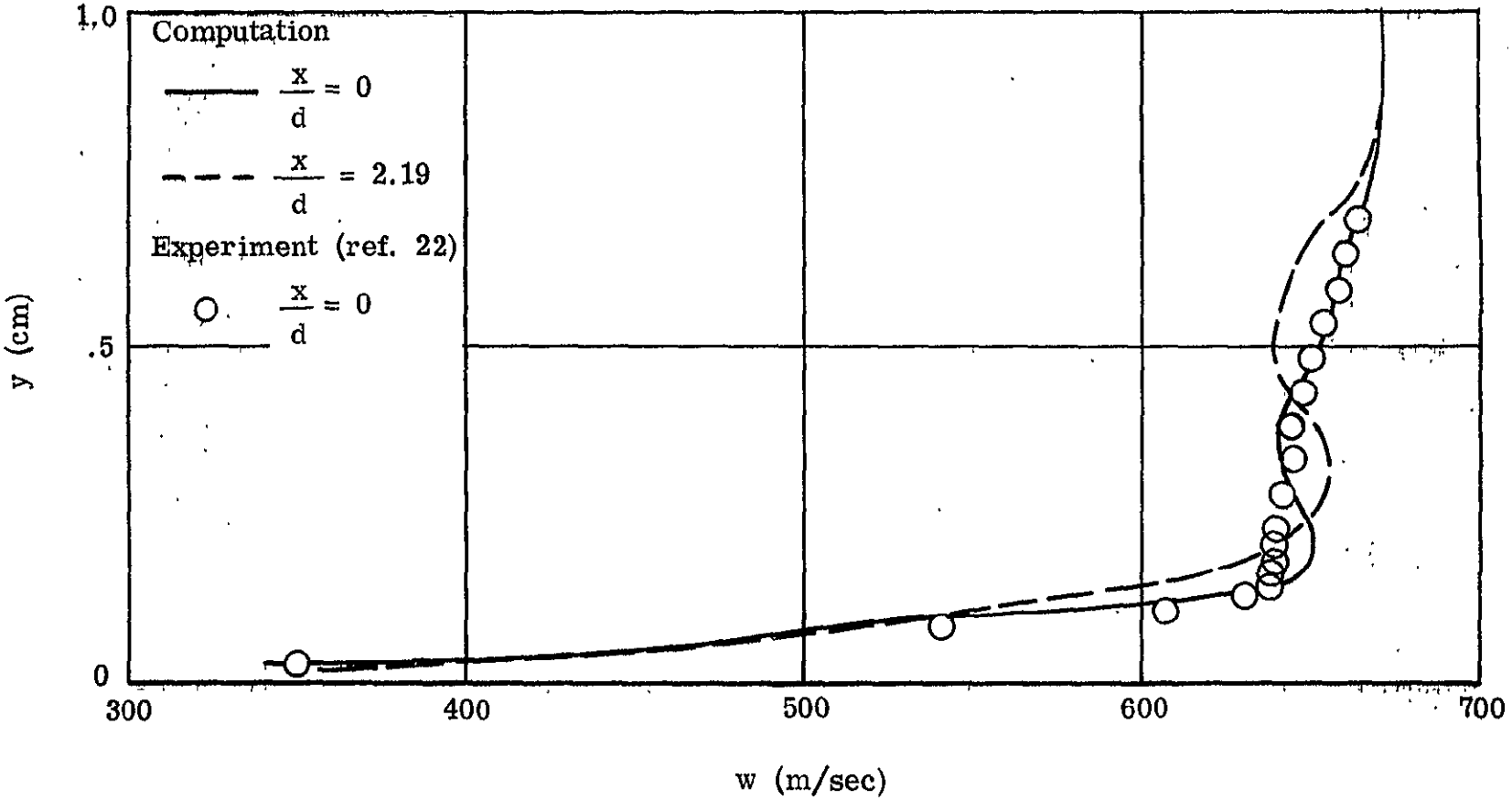

(a) Velocity.

Figure 16.- Comparison of computation with experiment.
($s/d = 6.25$, $(z-z_j)/d = 60$)

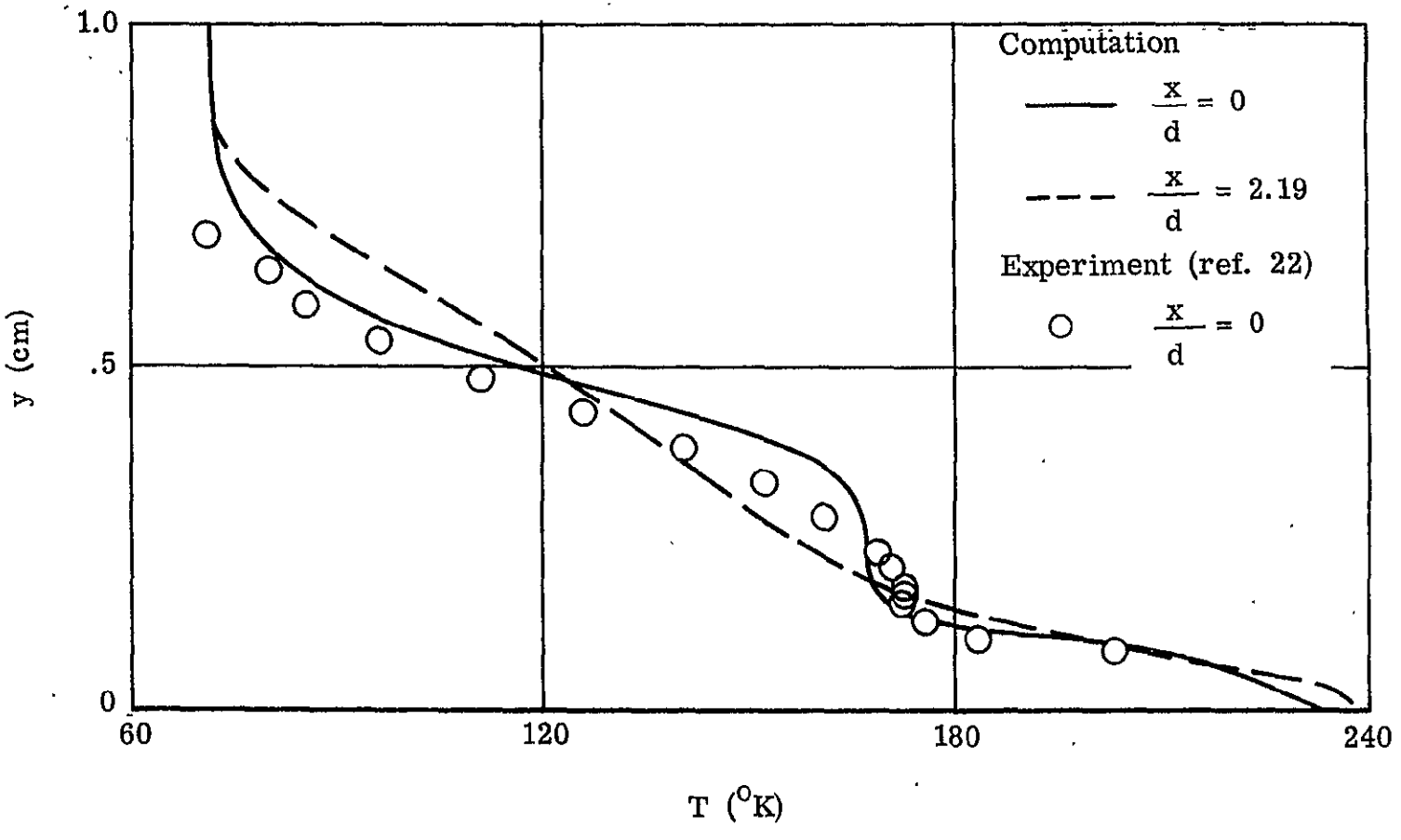

(b) Temperature.

Figure 16.- Continued.

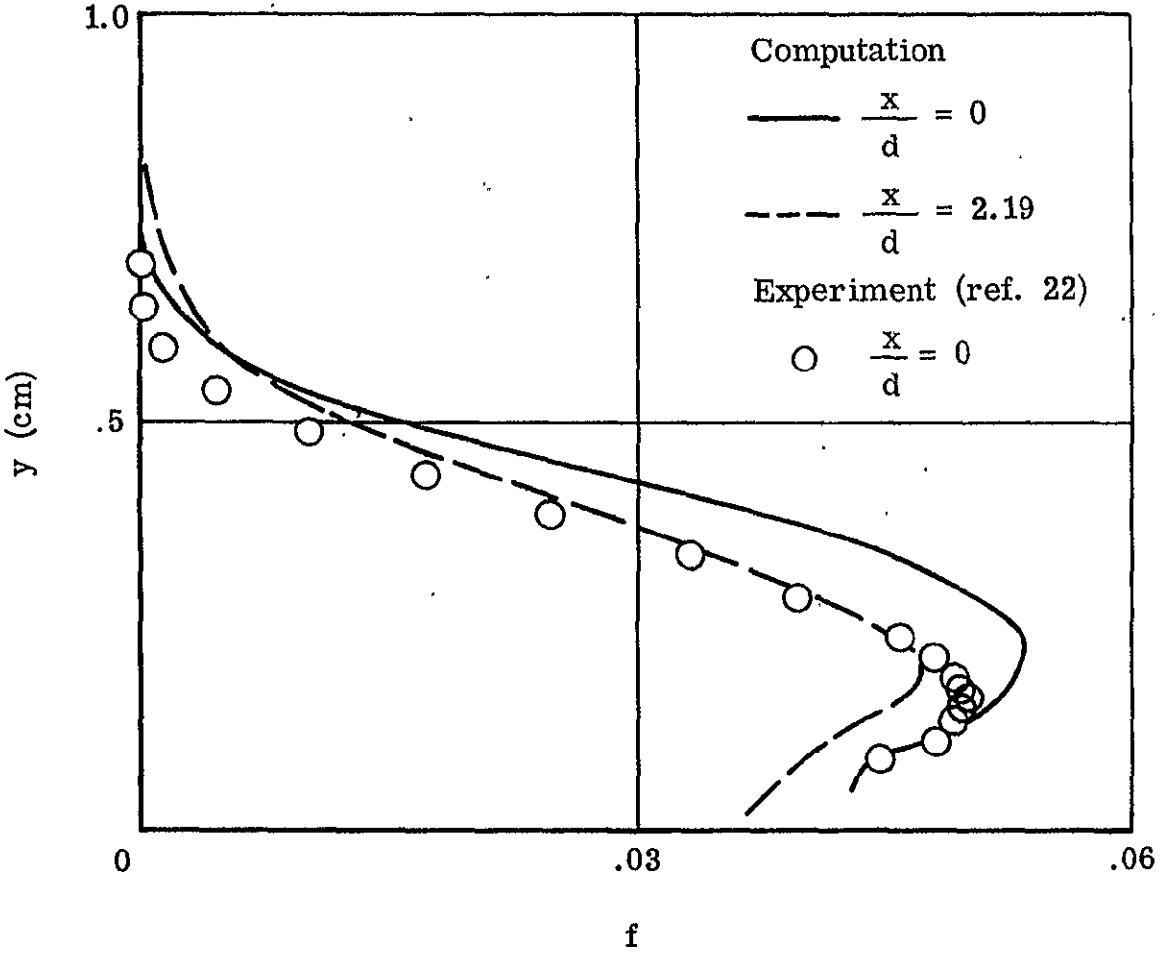

(c) Hydrogen concentration.

Figure 16.- Concluded.

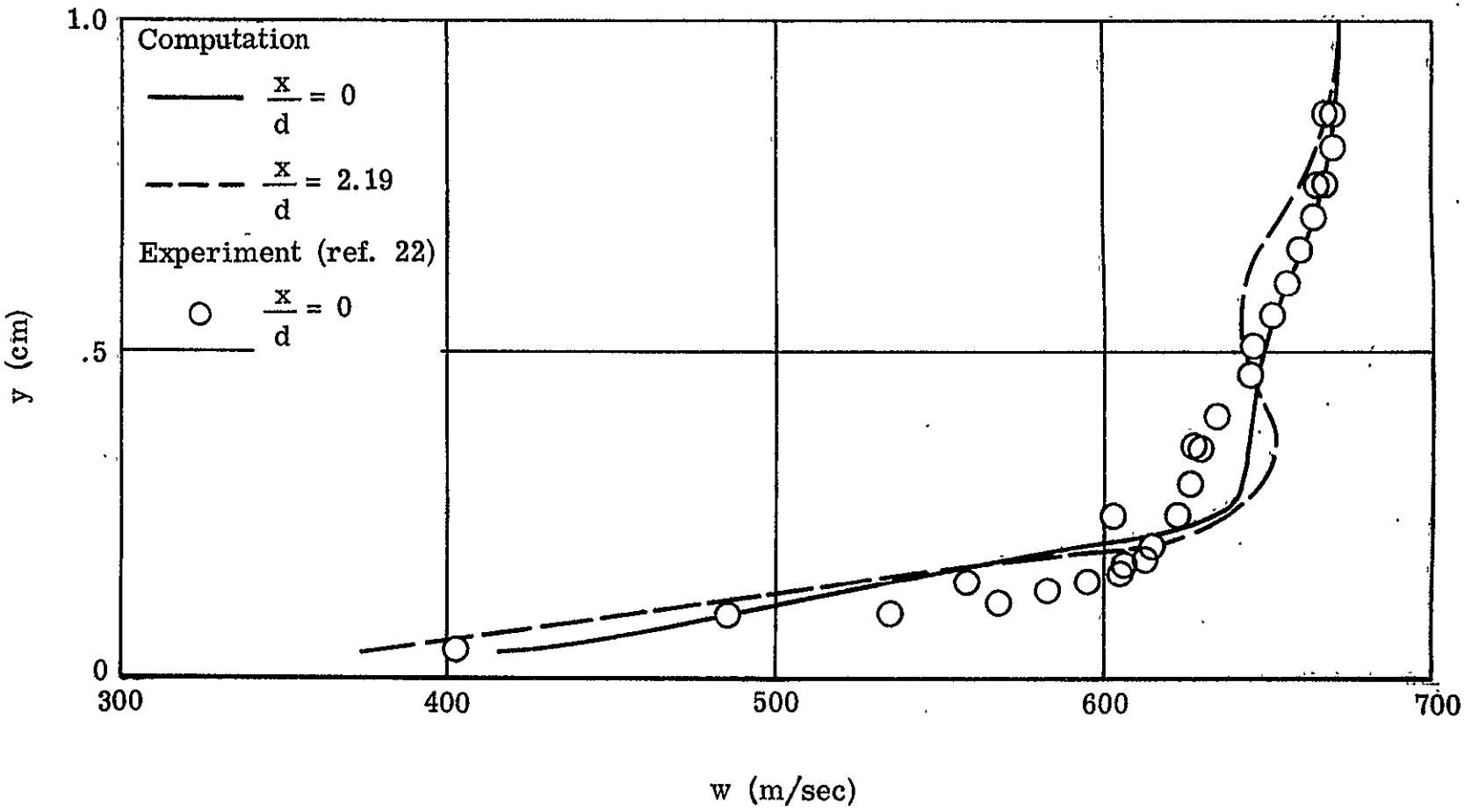

(a) Velocity.

Figure 17.- Comparison of computation with experiment.
($s/d = 6.25$, $(z-z_j)/d = 120$)

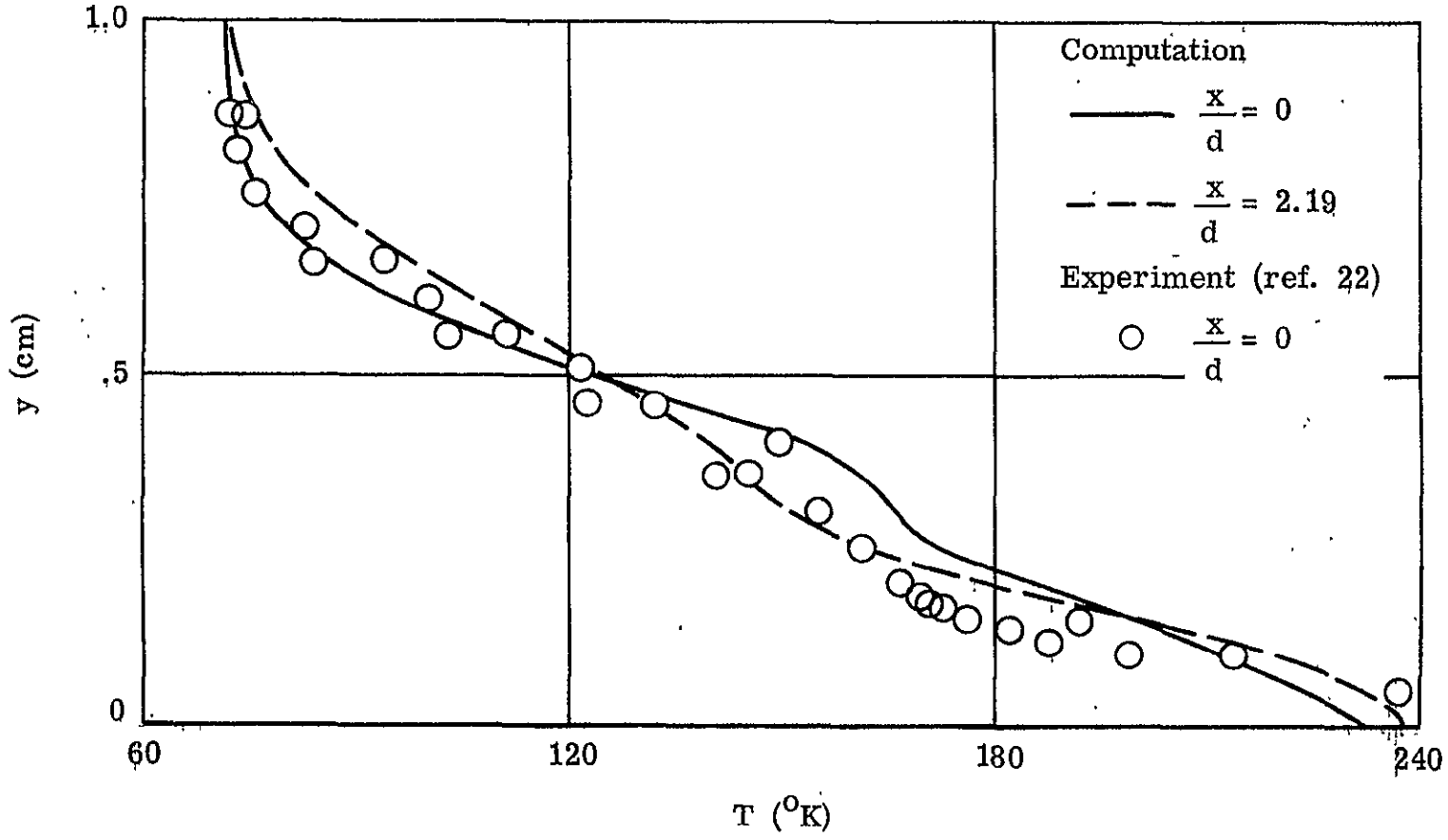

(b) Temperature.

Figure 17.- Continued.

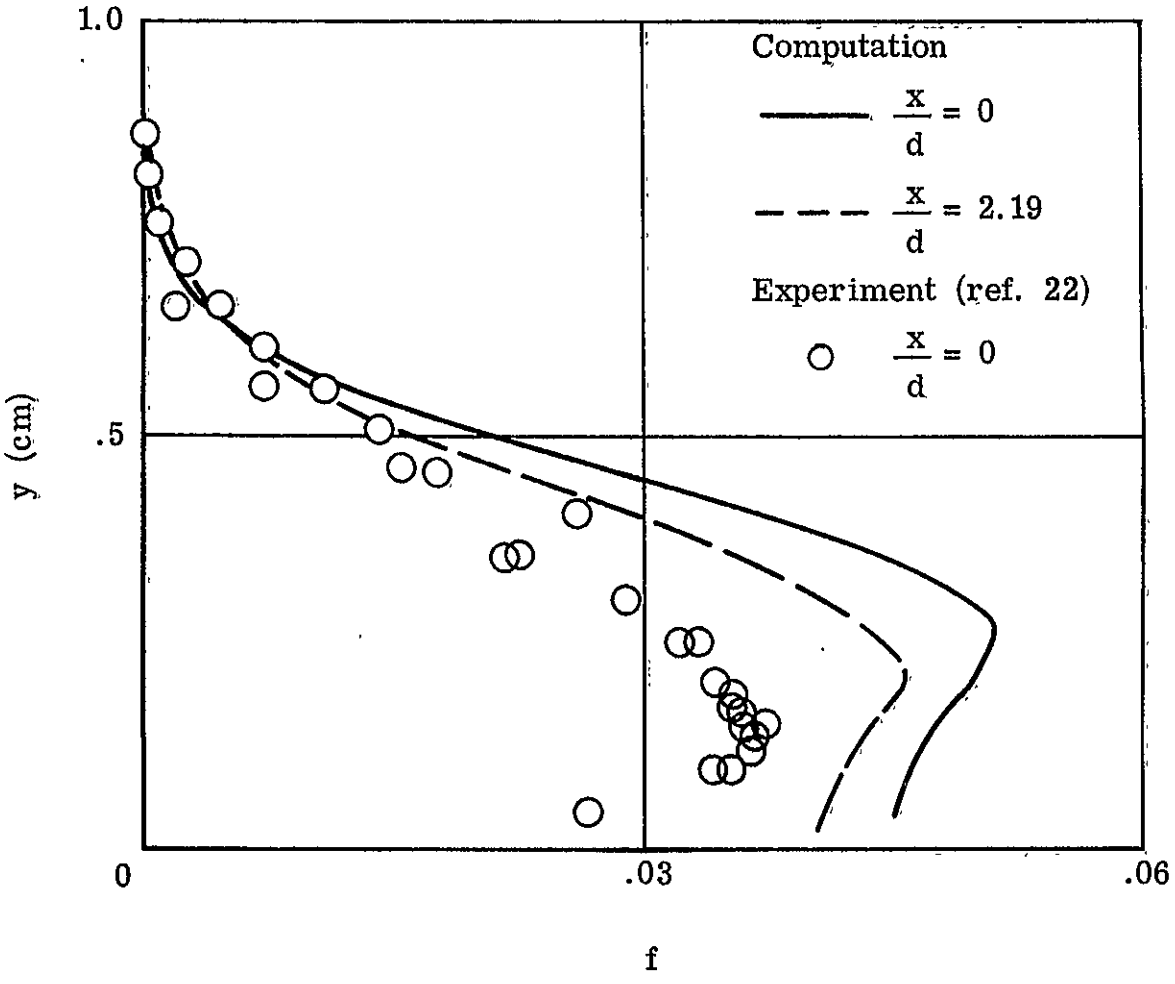

(c) Hydrogen concentration.

Figure 17.- Concluded.

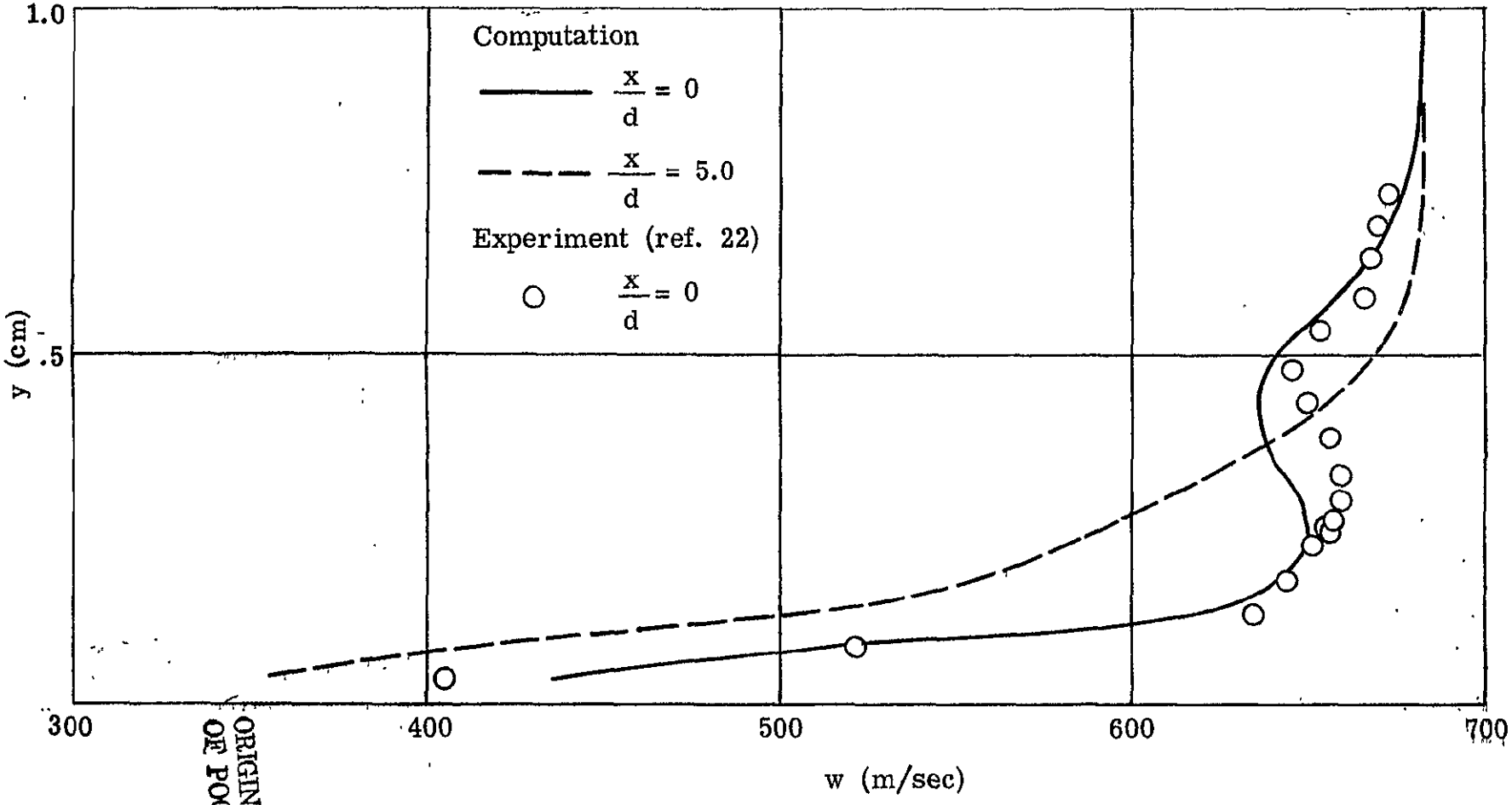

(a) Velocity.

Figure 18.- Comparison of computation with experiment.
($s/d = 12.5$, $(z-z_j)/d = 60$)

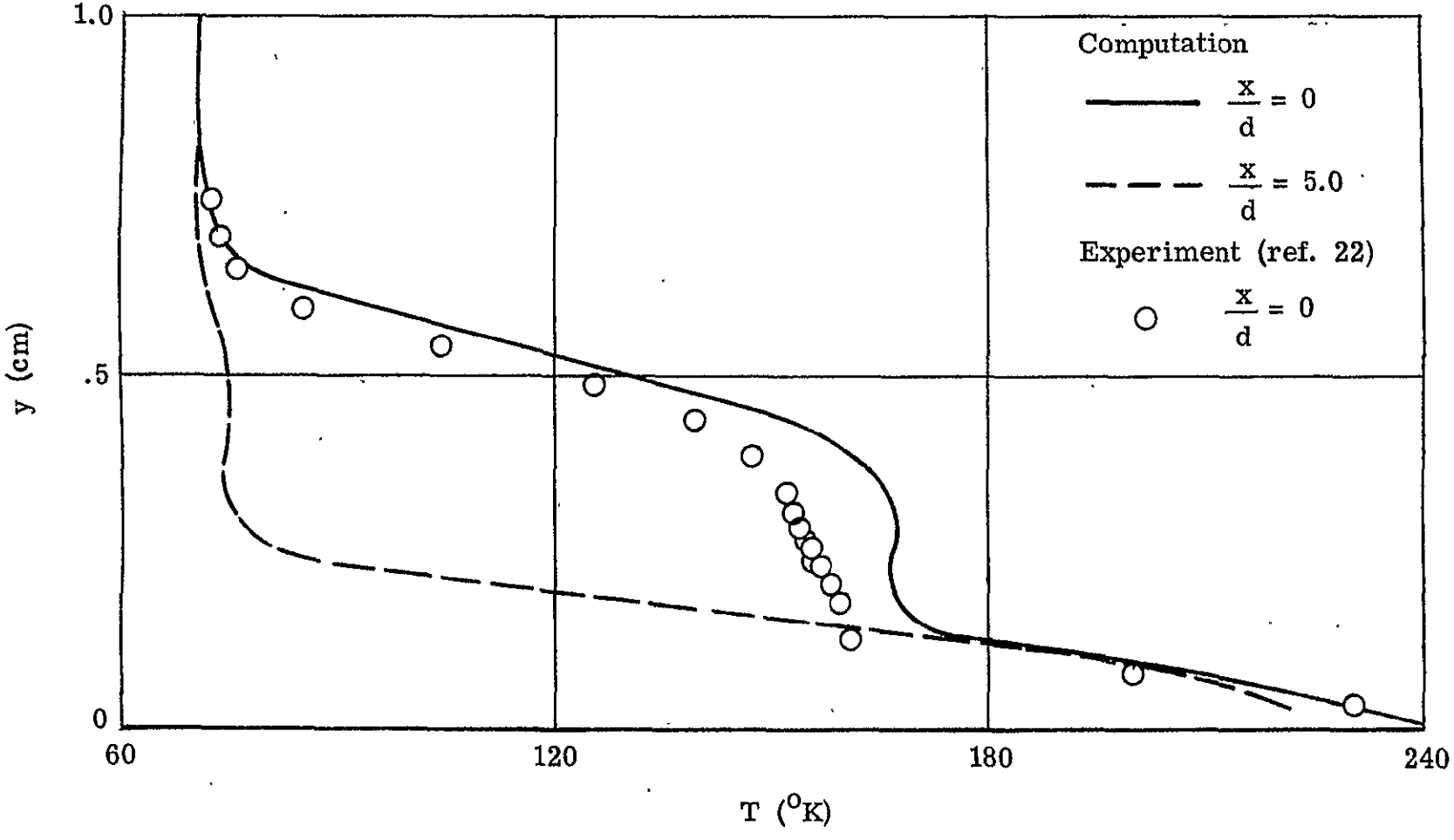

(b) Temperature.

Figure 18.- Continued.

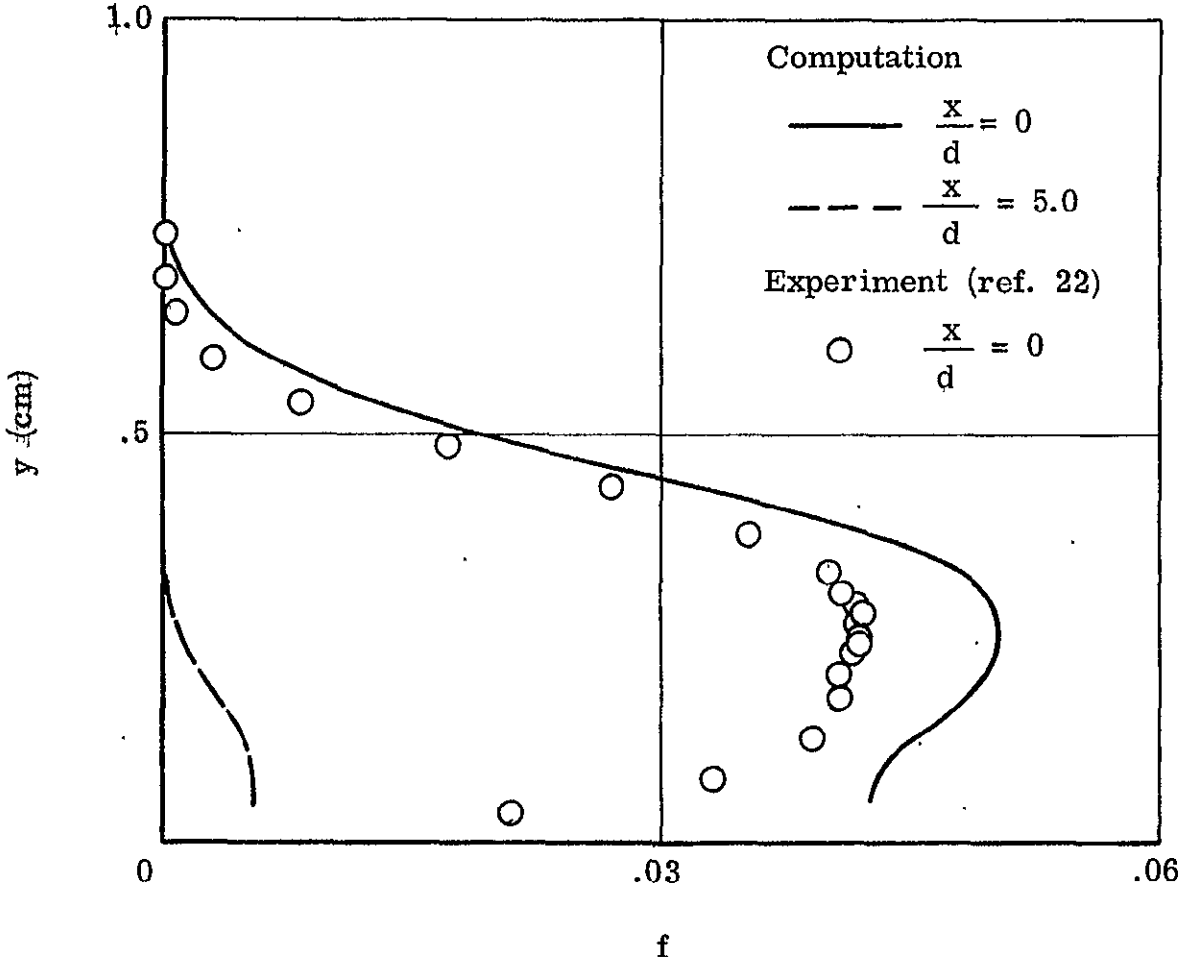

(c) Hydrogen concentration.

Figure 18.- Concluded.

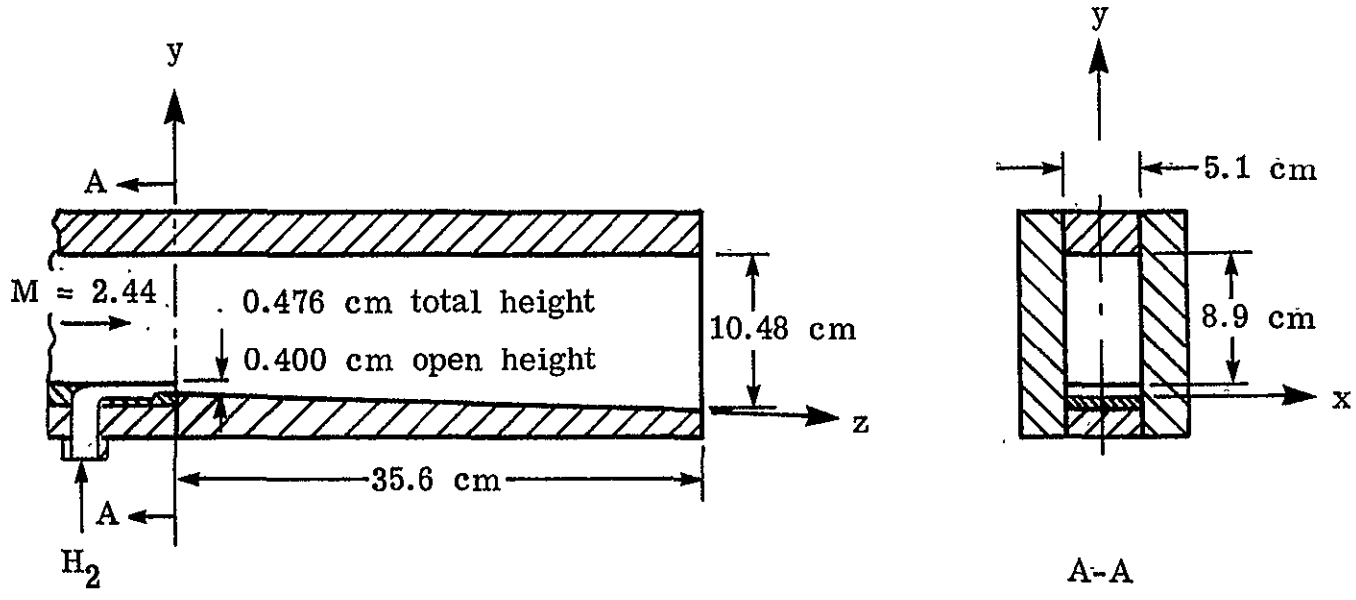

Figure 19.- Sketch of the test section of a combustor duct.

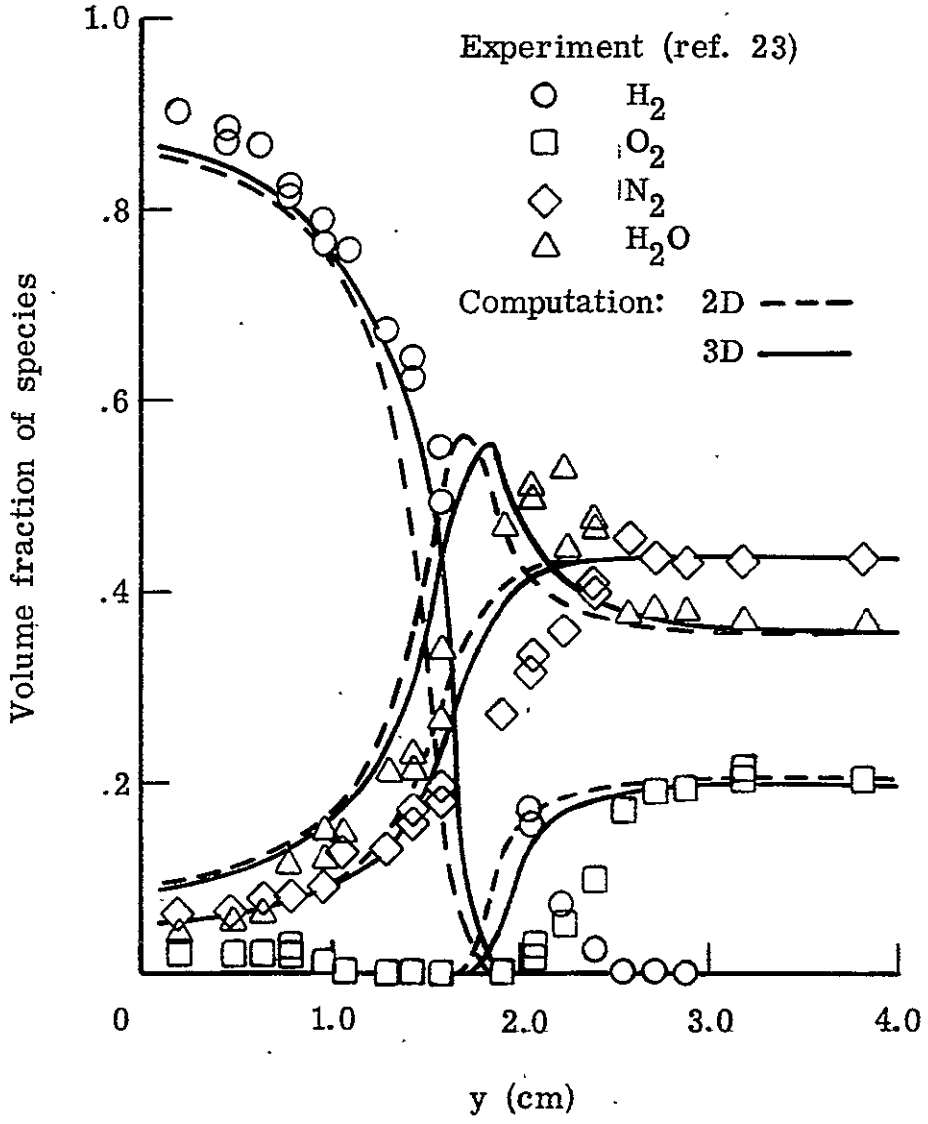

(a) Composition profiles.

Figure 20.- Comparison of computation with experiment. Supersonic combustion of hydrogen and vitiated air (z = 35.6 cm).

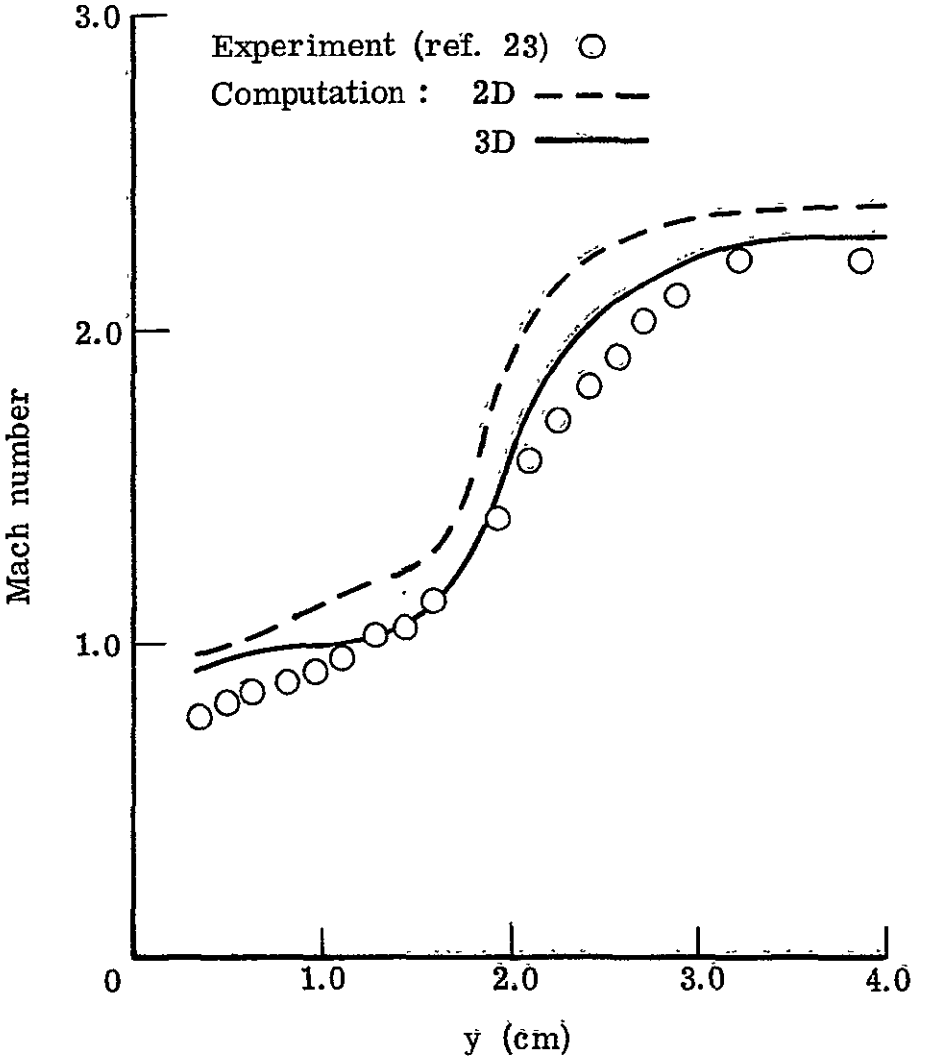

(b) Mach number profiles.

Figure 20.- Continued.

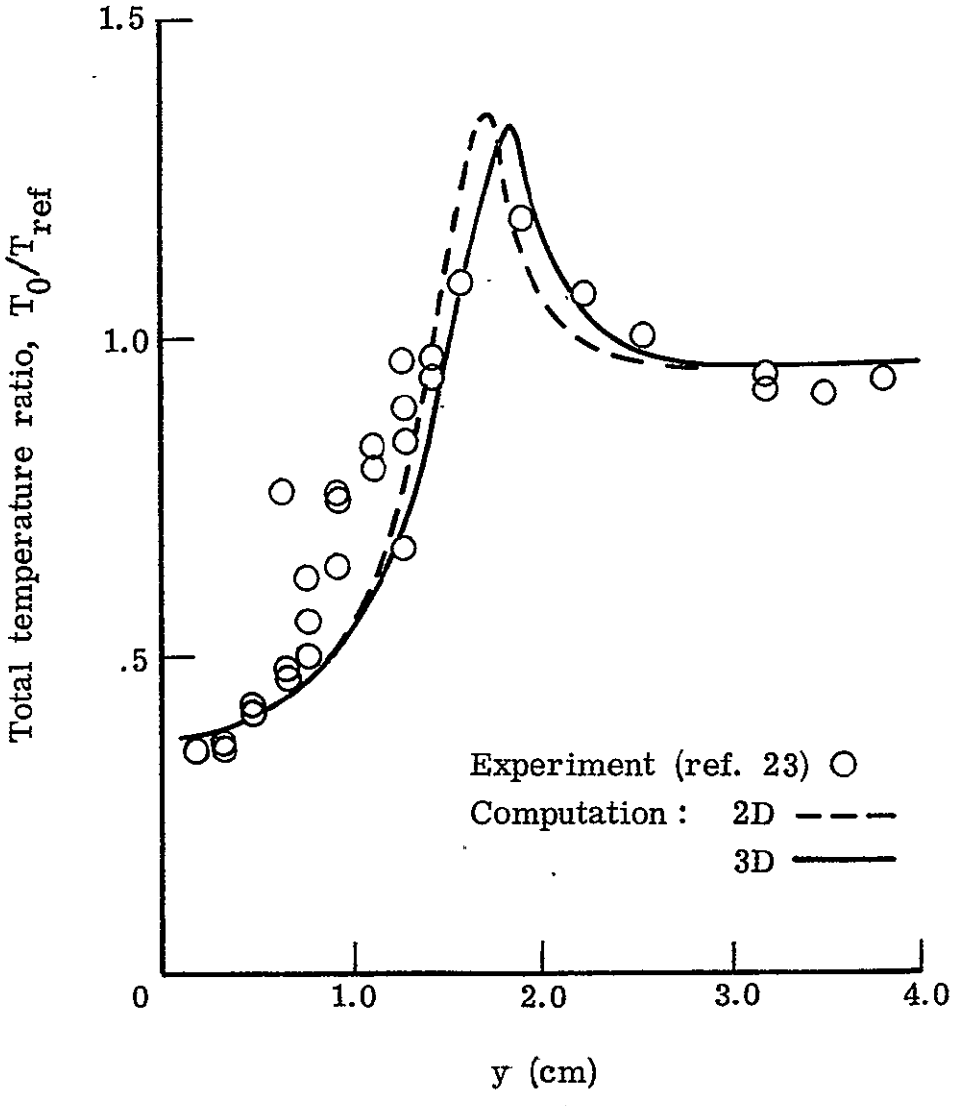

(c) Total temperature ratio profiles (T_{ref} = 2380 K).

Figure 20.- Continued.

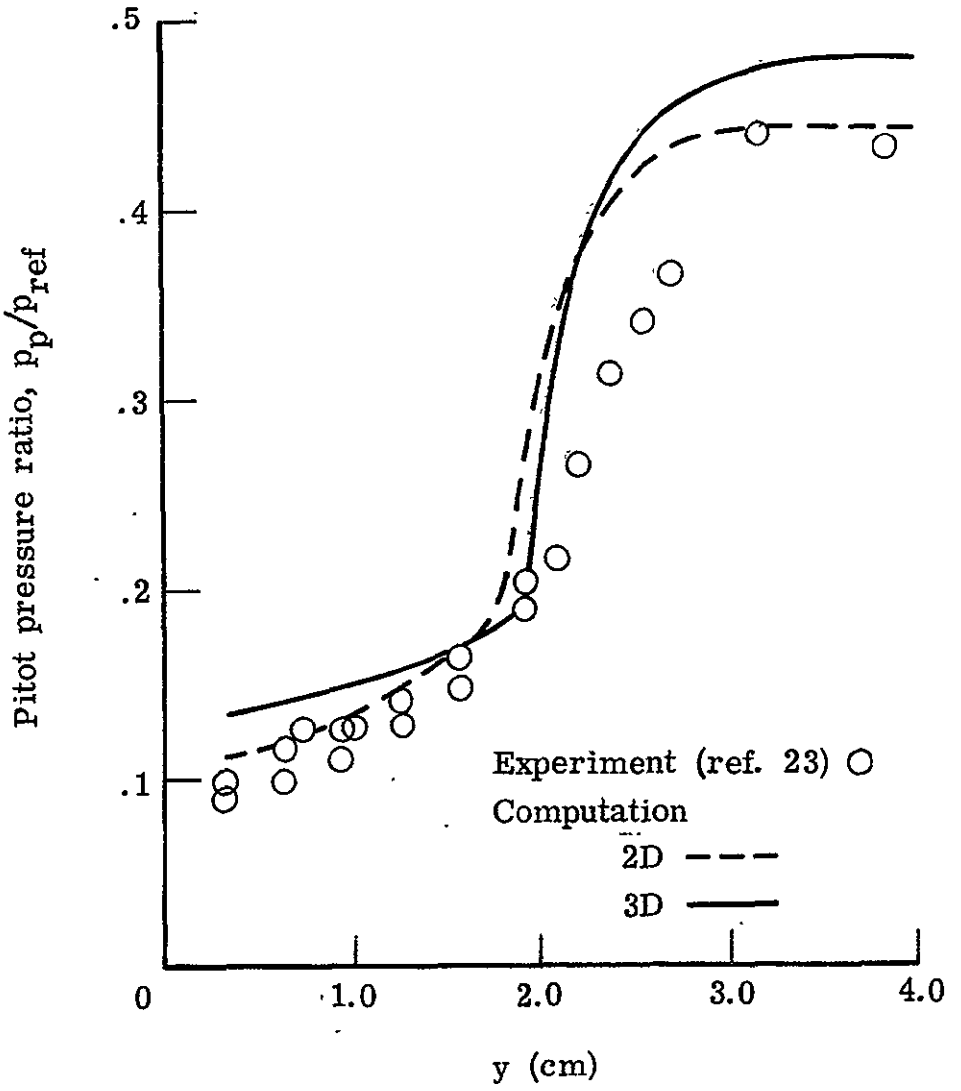

(d) Pitot pressure ratio profiles (p_{ref} = 17.1 × 10^5 N/m^2).

Figure 20.- Concluded.

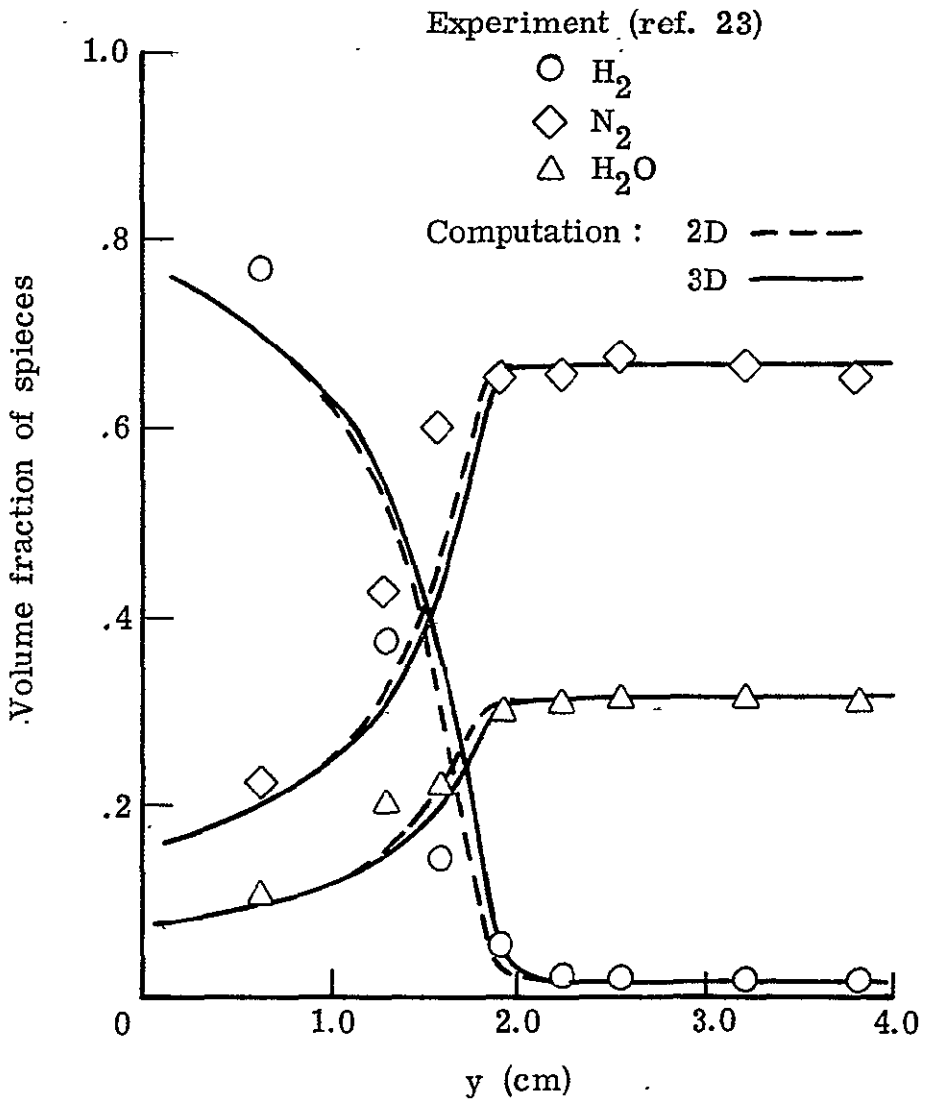

(a) Composition profiles.

Figure 21.- Comparison of computation with experiment. Turbulent mixing of hydrogen and inert gas (z = 35.6 cm).

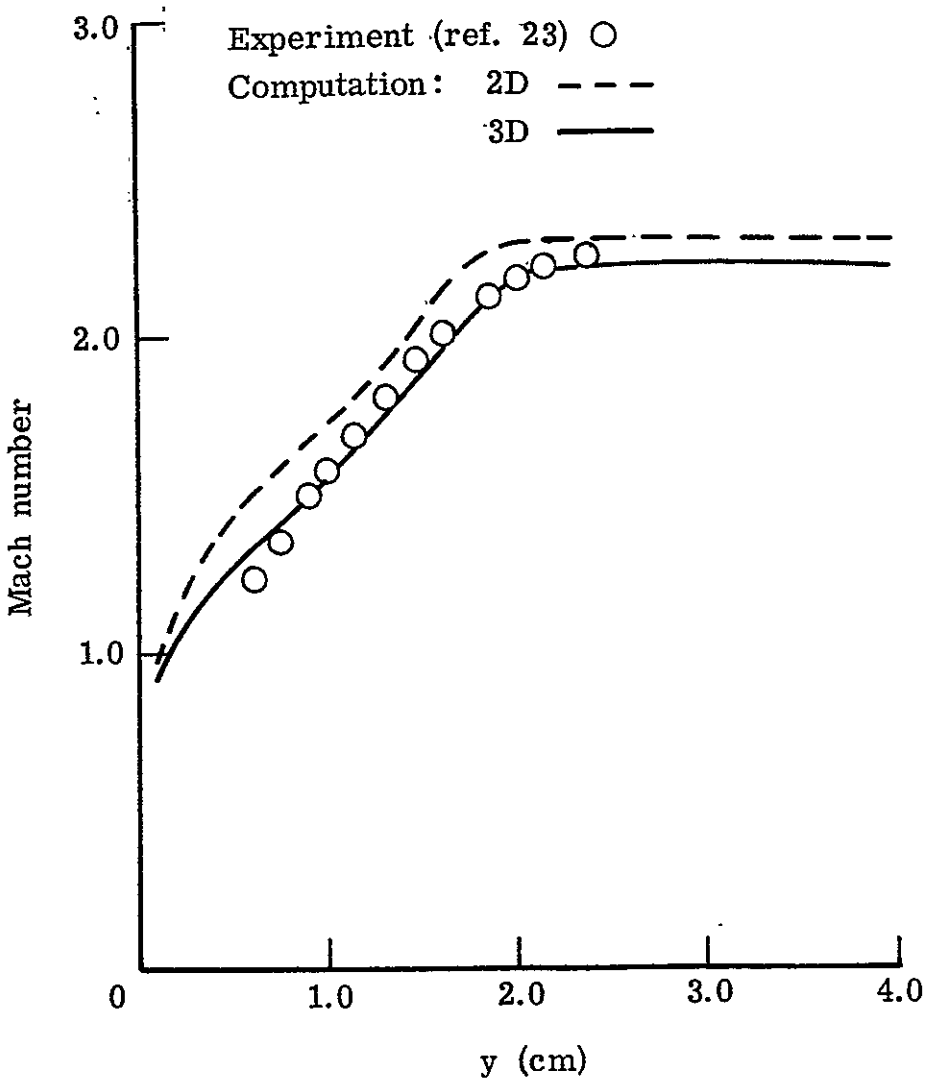

(b) Mach number profiles.

Figure 21.- Continued.

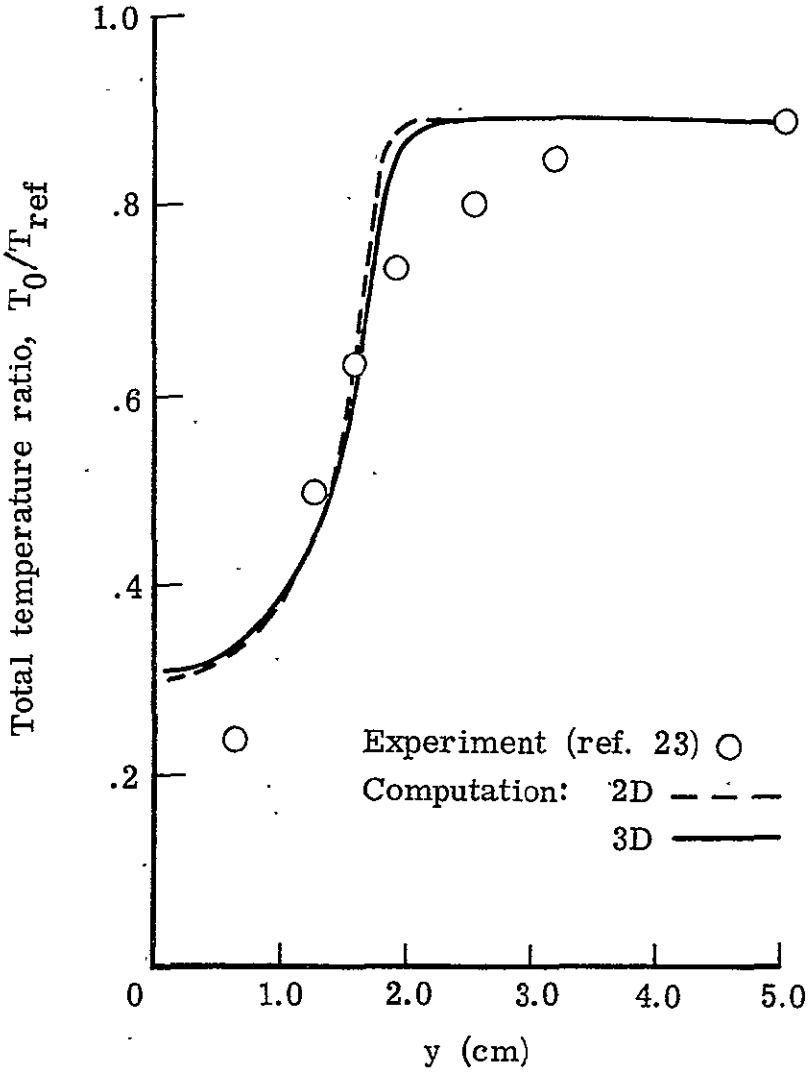

(c) Total temperature ratio profiles (T_{ref} = 2276 K).

Figure 21.- Continued.

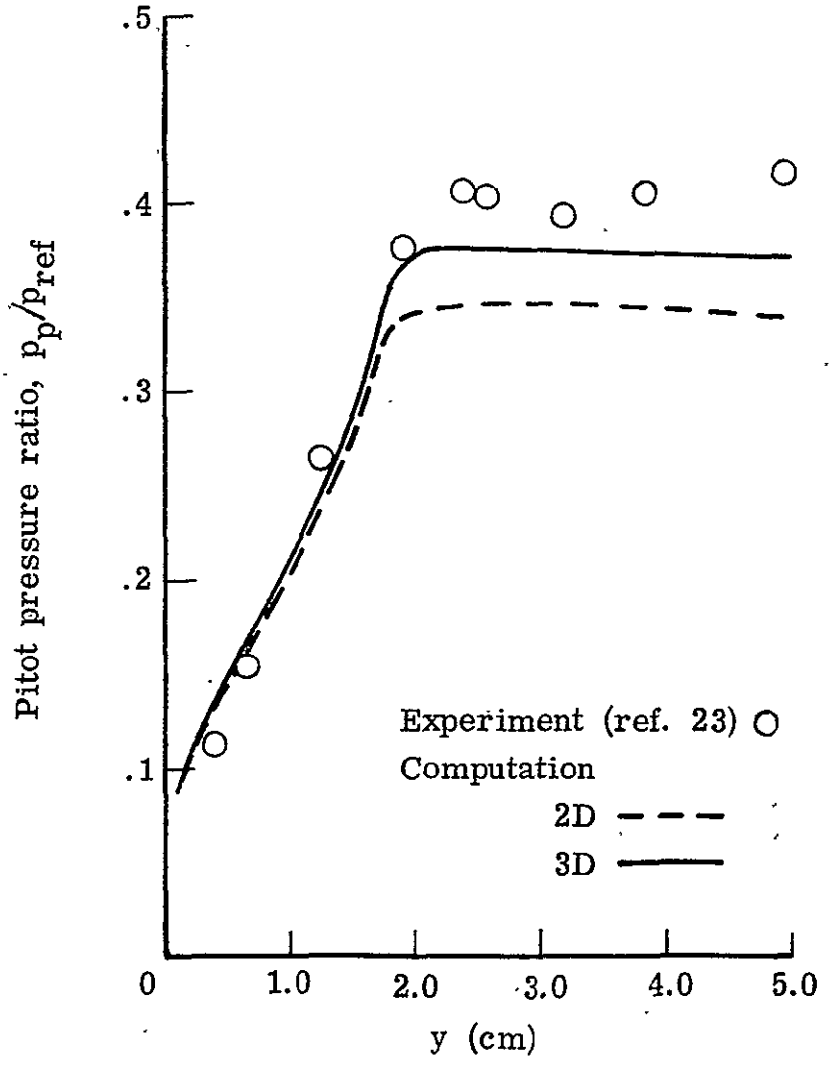

(d) Pitot pressure ratio profiles (p_{ref} = 18.5 × 10^5 N/m^2).

Figure 21.- Concluded.

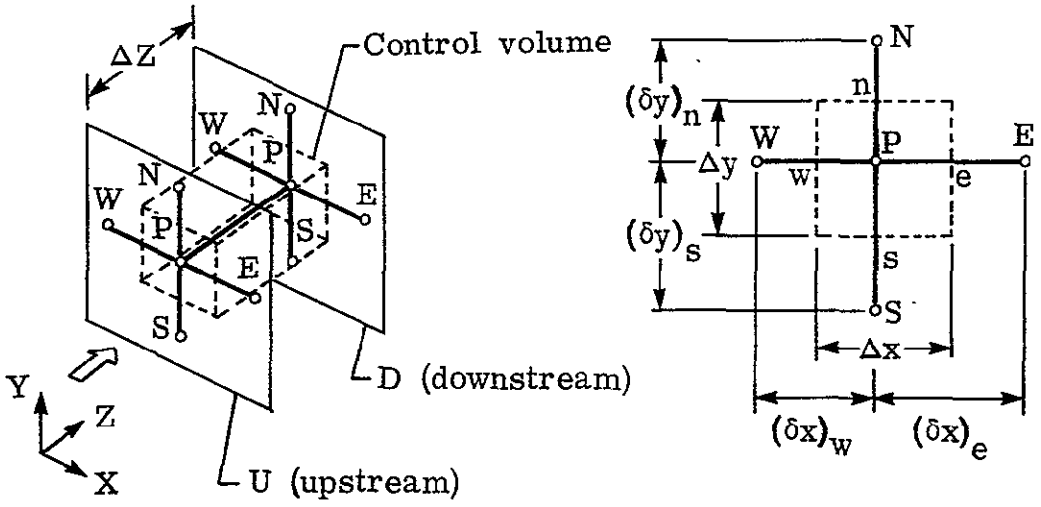

Figure 22. The control volume (ref. 4).

1. Report No.	2. Government Accession No.	3. Recipient's Catalog No.
NASA TM 74094		

4 Title and Subtitle	5 Report Date
EVALUATION OF THE THREE-DIMENSIONAL PARABOLIC FLOW COMPUTER PROGRAM SHIP	January 1978
	6. Performing Organization Code 3740
7. Author(s)	8. Performing Organization Report No.
Y. S. Pan	
	10. Work Unit No.
9 Performing Organization Name and Address	
NASA Langley Research Center Hampton, VA 23665	11. Contract or Grant No.
	13. Type of Report and Period Covered
12. Sponsoring Agency Name and Address	Technical Memorandum
National Aeronautics and Space Administration Washington, D.C. 20546	14. Sponsoring Agency Code

15. Supplementary Notes

This is the final release of special information not suitable for formal publication which serves the following need: To present the evaluation and capabilities of this three-dimensional turbulent reacting flow computer program.

16 Abstract

The three-dimensional parabolic flow program SHIP designed for predicting supersonic combustor flow fields is evaluated to determine its capabilities. The mathematical foundation and numerical procedure are reviewed; simplifications are pointed out and commented upon. The program is then evaluated numerically by applying it to several subsonic and supersonic, turbulent, reacting and non-reacting flow problems. Computational results are compared with available experimental or other analytical data. Good agreements are obtained when the simplifications on which the program is based are justified. Limitations of the program and the needs for improvement and extension are pointed out. The present three-dimensional parabolic flow program appears to be potentially useful for the development of supersonic combustors.

17. Key Words (Suggested by Author(s))	18. Distribution Statement
Three-dimensional parabolic flow Computer program evaluation Turbulent mixing Reacting flow Supersonic combustion	Unclassified - Unlimited

19. Security Classif. (of this report)	20. Security Classif. (of this page)	21. No. of Pages	22. Price*
Unclassified	Unclassified	86	$5.00

* For sale by the National Technical Information Service, Springfield, Virginia 22161